Bioprinting 28 (2022) e00232

Contents lists available at ScienceDirect

Bioprinting

journal homepage: www.sciencedirect.com/journal/bioprinting

3D bioprinted silk-reinforced Alginate-Gellan Gum constructs for cartilage regeneration

Juhi Chakraborty, Nilotpal Majumder, Aarushi Sharma, Sukanya Prasad, Sourabh Ghosh *

Department of Textile and Fibre Engineering, Indian Institute of Technology Delhi, New Delhi, 110016, India

ARTICLE INFO

Keywords:
Alginate
Gellan gum
Silk nanoparticles
Reinforcements
3D bioprinting
Printability

ABSTRACT

Even though a substantial amount of research has been undertaken in the domains of bioprinting over the last few years, various challenges exist concerning printability. One of the grave challenges in developing a bioink with superior printability is the constraint of material availability, cross-linking, and other processing parameters that should warrant adequate functioning post bioprinting. This study demonstrates the development of a multicomponent shear-thinning bioink comprising Alginate and Gellan Gum with good mechanical, biological, and adequate printing properties. The addition of two types of silk nanoparticles (SNP), native and regenerated, acted as a reinforcement to the bioink, enhancing its printability. Additionally, silk fibroin solution was added to the bioink that served as a control apart from SNP. The addition of cationic SNP (native) to the anionic polymer mixture of Alginate-Gellan Gum exhibited a remarkable increase in the viscosity, storage modulus and mechanical property compared to the other experimental sets. Molecular characterization studies involving Real-Time PCR, gene expression, immunofluorescence, and histology analysis depicted enhanced chondrogenesis in the bioprinted construct containing the silk fibroin solution. The incorporated SNPs resulted in extracellular matrix secretion towards chondrogenesis of articular cartilage. Taken together, the method's broad applicability is likely to propel the field closer to the goal of precision bioprinting.

1. Introduction

Over the last couple of years, a remarkable volume of research has been directed in the domains of bioprinting. However, various challenges exist concerning the printability of bioink [1,2]. One of the grave challenges in developing a bioink with superior printability is the constraint of material availability, rheology, cross-linking, and other processing parameters that should warrant adequate functioning post bioprinting. In extrusion-based bioprinting, achieving good printability, precise printing fidelity, and mechanical stability is still cumbersome. The bioink material should maintain the imparted shape and uniformly protrude through the nozzle during extrusion. However, sometimes they deform or start flowing during extrusion, indicating nonuniformity in printability.

A printable polymeric system can be determined by the rheological assessment of the biomaterial in terms of its shear-thinning behavior and shear recovery. An ink with high viscosity can be extruded easily from the nozzle if it has a high shear-thinning property which warrants post-printing cell viability. On the contrary, high shear recovery rate plus yield stress permits it to keep hold and retrieve its shape post extrusion phase, ensuring shape fidelity of the printed structure [3]. One of the major problems often encountered using hydrogel material is the shrinkage of the scaffold post-printing, which should be maintained to achieve shape fidelity [4]. This further gets aggravated due to weak printing accuracy and poor mechanical properties. This makes it challenging to process them into structural materials further and makes them vulnerable to collapse [5,6]. Along these lines, several attempts have been carried out to regulate the rheological characteristics of the hydrogel-based bioinks and maintain their shape fidelity post-printing. Developing a composite material scaffold by combining the polymer bioink with fillers or reinforcements can potentially solve this problem.

Hydrogel-based bioinks exhibit excessive fluidity before cross-linking, which may hinder achieving a good shape fidelity. The printed cell-laden scaffolds are expected to have the least volume shrinkage and should provide adequate mechanical properties post crosslinking [7]. However, achieving these requirements simultaneously by a single component hydrogel is cumbersome. For instance, Alginate (Alg), polysaccharide-derived brown algae, has been long utilized for tissue

* Corresponding author.
E-mail address: Sourabh.Ghosh@textile.iitd.ac.in (S. Ghosh).

https://doi.org/10.1016/j.bprint.2022.e00232
Received 7 May 2022; Received in revised form 26 July 2022; Accepted 26 July 2022
Available online 10 August 2022

engineering purposes [8]. Alg can be cross-linked with multivalent cations [9]. Although sodium alginate can result in a mechanically durable scaffold by undergoing rapid gelation with Ca^{2+}, it cannot overcome the problem of substantial volume shrinkage at the time of gelation, resulting in a scaffold with inadequate scaffold stiffness. On the contrary, Gellan Gum (GG), an anionic polysaccharide produced by the bacteria *Sphingomonas paucimobilis* displays insignificant deformation during gelation since the hydrogel formed has adequate stiffness but lacks toughness [10]. When combined, GG reduces the deformation of the construct due to its stiff network, whereas Alg maintains the toughness of the structure and prevents the construct from any breakage. In addition, the cell culture media enable further cross-linking of GG, which decelerates the degradation rate of the printed construct when placed in cell culture media [11]. Akkineni et al. reported 3D printed Alg-GG constructs with increased printability and structural stability [12]. In another study, Alg and GG-based bioink were used where GG imparted the essential shear thinning and the recovery properties crucial to printing due to its cooling-induced physical gelation property [13]. This study added commercially available Bio-Cartilage particles (cartilage ECM particles) to the Alg-GG bioink. A comparison was made by adding hydroxyapatite to exhibit printability independent of particle type. The bioink with the commercial ECM particles aided in chondrocyte proliferation and enhanced deposition of cartilage matrix proteins in the presence of transforming growth factor β-3. This study manifested that the ECM particles can be restored to some extent to de novo bioprinted cartilaginous structure. In a follow-up study, Lee et al. added cationic-modified silica nanoparticles (NPs) in the Alg-GG bioink, which resulted in high printability and 3D printing fidelity [14]. There was a significant improvement in shear-thinning properties, zero-shear viscosity, storage modulus, and mechanical strength as silica NPs could reversibly cross-link both anionic polysaccharides, Alg and GG. Mechanical enhancement was also achieved that was dependent on size, concentration, and surface chemistry. Keeping this in mind, in the current study, we attempted to develop a functionalized, reinforced Alg-GG bioink to enhance the chondrogenic potential of the bone marrow-derived Mesenchymal stem cells (MSCs).

Many organic/inorganic composite materials, such as fumed silica[15] and laponite[16] combined with polymeric solutions, improved the bioink's shear-thinning property and provided zero shear viscosity. Milled silk particles have been explored to reinforce scaffolds, considering their exceptional properties and cytocompatibility [15]. For example, Vyas et al. incorporated silk microparticles into polycaprolactone scaffolds that imparted potent mechanical reinforcement and enhanced the degradation rate and cell proliferation, displaying a high prospective for bone tissue engineering applications. Furthermore, the rheological analysis showed that the incorporation of silk microparticles improved the shear-thinning property and storage modulus of the material [16]. Thus, it can be inferred that the NP part of the ink plays a crucial role in regulating the mechanical properties and printability of such formulated nanocomposite bioinks. Considering these properties, our question is, if we use silk nanoparticles (SNPs) from *Bombyx mori* as reinforcements, would it be able to modulate the printability? To a large extent, the structure of the SNPs depends on their processing method. However, the influence of the processing method on NP fabrication, characteristics, and its secondary structure constitution is mainly unknown. Normal silk fibers that are directly cryomilled give rise to native SNPs, whereas the extensive processing steps such as degumming, dissolution, etc., render regenerated SNPs [17]. It is reported that, apart from the surrounding environment, pH, and salt concentration, the secondary conformation structures of native SNPs are strongly influenced by the mechanics such as drying and shear stress [18]. Adding these SNPs to a bioink can have a contrasting effect on the secondary conformation and surface charge. These factors may vary when silk fibroin (SF) solution is added instead of SNPs. Depending upon the processing conditions, particularly pH values, zeta potential measurements of silk particles produced from regenerated solution were found to vary from 26.3 mV (pH 4) to 46.0 mV (pH 9) [19]. Hence, we thought to utilize the ability of developed charged SNPs to impart functionality to the bioink. It would be fascinating to determine how the zeta potential value of various SNPs modulates the printability, using the SF solution as a control.

In this study, we report the development of a multicomponent shear-thinning bioink comprising Alg and GG with good mechanical, biological, and adequate printing properties. Further, we added two types of SNPs, native and regenerated, which act as a reinforcement to the Alg-GG bioink. Additionally, SF solution was added to the bioink that served as a control apart from SNP. This is, to our knowledge, the first study of its kind elucidating the amalgamation of different SNPs and SF solutions with a multicomponent bioink toward chondrogenic differentiation of MSCs. Precisely we would like to focus on the following questions in our study:

1. Will there be any difference in crystallinity, and particle size, if silk fibers are directly cryomilled (native silk) instead of dissolution and aggregation (regenerated silk), followed by cryomilling? Besides, how would these changes modulate the SF secondary conformations and surface charge properties?
2. If we can incorporate SNPs from native silk or regenerated silk, within the Alg-GG bioink, what will be its impact on the rheology and printability?
3. If we then encapsulate stem cells (MSCs) within the Alg-GG ink with native, regenerated SNPs and SF solution, how will these conditions affect the gene expression or protein production pattern?

2. Materials and methods

2.1. Preparation of SF nanoparticles and the solution

Bombyx mori cocoons were benevolently provided by Central Silk Technological Research Institute (Central Silk Board), Bangalore, Ministry of Textiles, Government of India. Briefly, 5 gm of silk cocoons were chopped into small pieces and boiled twice for about 20 min in 0.02 M Na_2CO_3 to remove sericin. This was followed by rinsing 7–8 times in deionized water to remove the alkali from the degummed fibers. The fibers were dried overnight in an incubator at 37 °C [20,21]. After drying, the fibers were (i) directly cryomilled (Retsch GmbH, Germany) to obtain native SNPs (ii) dissolved in 9.3 M LiBr solution (SRL Pvt. Ltd., India) for 4 h at 60 °C. The resultant SF solution (hereafter termed Silk sol.) was dialyzed against deionized water using a Slide-a-Lyzer dialysis cassette (MWCO 3500, Pierce) for 48 h to remove the lithium bromide. The fibroin polymers crystallized inside the cassette were cryomilled to obtain regenerated SNPs, whereas (iii) the dialyzed solution without crystallization resulted in 5% w/v of SF aqueous solution [22].

2.2. SF cryogenic grinding

The cryogenic grinding was done using a cryomill (Retsch, Switzerland, 25 ml grinding jar, 15 mm Ø grinding balls) which consisted of several cycles, (i) the precycle that allowed the sample to reach the temperature of the liquid nitrogen injected into the CryoMill's chamber i.e., −196 °C, (ii) the grinding cycle, the step during which the container was agitated. The sample was placed in the container with several stainless steel (or tungsten carbide) grinding balls. They were milled between the wall and the steel spheres or several spheres (iii)The intermediate cycle ensures that the sample returns to the liquid nitrogen's temperature regularly. The container was shaken but not as strong as during the grinding cycle.

The frequency of agitation was as follows, Precycle: 10 min; grinding cycles (*3): 30 Hz, 5 min; Intermediate cycles (*2): 5 Hz, 3 min.

2.3. Characterization of particles

2.3.1. Zeta potential and dynamic light scattering

The surface zeta potential and average particle size of both the native and regenerated SNPs were determined by dynamic light scattering (DLS) Zetasizer Nano ZS, 90 (Malvern, UK) instruments. The samples were prepared in deionized water, and the concentration of the colloidal solution was 0.5 mg/ml, which was ultrasonicated for 30 min amplitude with an on and off pulse rate of 5 min, resulting in a uniformly dispersed solution. The obtained equi-dispersed solution was then used to determine surface zeta potential and particle size.

2.3.2. Attenuated total reflectance-fourier transform infrared spectroscopy (ATR-FTIR)

The ATR-FTIR spectra of native and regenerated SNPs were calculated using an Alpha-P spectroscope (Bruker, USA) in absorbance mode, with a spectral resolution of 4 cm^{-1}, 50 scans, and then the spectra were compared. All scans were performed in the same location on the same piece of material for each sample. To prevent overlapping the spectrum, FTIR spectra of the materials were produced in absorbance mode from 1200 to 1750 cm^{-1} wavenumbers with an offset value of 0.10.6 (a.u.). OriginPro 8.5 (OriginLab Corporation, Northampton, MA, USA) was used to generate Fourier self-deconvolution (FSD) spectra described elsewhere [23]. In the amide I region between 1595 and 1705 cm^{-1}, Gaussian profiles were used to fit the FSD FTIR spectra. The amide I range is divided into different secondary conformations, such as 1616–1637 cm^{-1} and 1695–1705 cm^{-1} for β-sheet, 1638–1655 cm^{-1} for random coil, 1656–1663 cm^{-1} for α-helices, and 1663–1695 cm^{-1} for β-turns. The frequency ranges of the silk β-sheet fraction, determined by the integral of Gaussian profiles (termed "bands") [24], are divided by the frequency ranges of the silk β-sheet. The ratio of these bands to the total amide I bands [25] was used to calculate the secondary conformation fractions.

2.4. Preparation of the acellular bioinks and their cross-linking

All the different types of inks were prepared in a solution involving 300 mM glucose (Sigma-Aldrich) and 20 mM (4-(2-hydroxyethyl)-1-piperazineethanesulfonic acid) (HEPES, Sigma-Aldrich) at pH 7.4. The control ink was prepared by adding Alg- 1% (w/v) and GG- 1% (w/v) to the above-prepared solution and kept in the magnetic stirrer at 90 °C and 300 rpm for 1 h. The resultant mixture was then strongly mixed with a spatula until it cooled down to room temperature. The post-processing step involved passing the ink through two plastic syringes (Medmix Systems AG, Risch-Rotkreuz, Switzerland) for 5 min, connected via a lure connector to remove agglomerations. Inks containing SNPs were prepared by mixing 15 mg/ml of the SNPs (native and regenerated) powder with the control Alg-GG hydrogel via the connector. Lastly, an equivalent amount of silk solution was added to the control ink. Finally, the ink was centrifuged at around 100 rcf for 3–5 min to remove air bubbles from the gel. Post-printing stabilization of the Alg-GG structures was achieved by cross-linking with 100 mM $CaCl_2$ (Sigma Aldrich) solution for 30 min [26].

2.5. Rheological characterization of the bioink

The shear-thinning behavior of the developed ink, i.e., Alg-GG ink containing native, regenerated SNP, and Silk sol., was assessed using a rotational Rheometer (MCR 302, Anton Paar) by applying a shear rate sweep using a plate-plate configuration at 25 °C. The diameter of the zone of the measuring tool in contact with the sample was 25 mm, and the gap between the two plates was set at 0.5 mm, defining a volume of sample to be inserted of 200 µl. The inks were freshly synthesized and directly used for the experiment. The samples being tested are GG, Alg, Alg-GG, Alg-GG-Silk sol., Alg-GG-15 N SNP, Alg-GG-30 N SNP, Alg-GG-45 N SNP, Alg-GG-15R SNP, Alg-GG-30R SNP, Alg-Gg-45R SNP, (where, R SNP-regenerated SNPs and N SNP- native SNPs). The flow behavior was evaluated in the shear rate range of 0.1–1000 s^{-1} to analyze the effect of shear on different inks at 22 °C. The detailed composition of the inks is mentioned in Table 1.

The dynamic storage (G′) and loss modulus (G″) of all the blends were measured in oscillatory mode at 25 °C. In the amplitude sweep measurement, the materials were tested for strain values of 0.1–100% by keeping the frequency constant at 1 Hz. In the frequency sweep measurement, materials were tested from 0.1 to 100 Hz frequency range by keeping the strain constant at 2%.

2.5.1. Yield stress and shear recovery

The yield stress was calculated by plotting the viscosity vs. shear stress curve in Origin 2021.

The shear recovery of the multicomponent Alg-GG biomaterial with the chosen concentration of regenerated and native SNPs was carried out at a fixed frequency of 1 Hz and 25 °C temperature. The material was subjected to a shear rate of 0.001 s^{-1} for 2 min (before extrusion), followed by a shear rate of 200 s^{-1} for 1 min (during extrusion), and finally, a shear rate of 0.001 s^{-1} (post extrusion). The shear viscosity vs. time graph was plotted in Origin 2021 to calculate the percentage recovery.

2.6. Mechanical testing of the hydrogels

2.6.1. Tensile testing

The tensile property of the material was evaluated using a Tinus Olsen Universal Testing Machine. The Alg-GG films incorporated with SNPs and Silk sol. were cut into equal dimensions of 40 mm × 10 mm with a thickness of 0.42 mm (Alg-GG-15R SNP), 0.13 mm (Alg-GG-15 N SNP), and 0.15 mm (Alg-GG-Silk sol.) respectively. The test was carried out at a 10 mm/min speed with a load of 10 N. The modulus was calculated from the slope of the stress-strain curve, whereas the tensile strength was evaluated at the fracture point (n = 3).

2.6.2. Compression testing

The compression property of the hydrogel was determined using an Instron Universal Testing Machine. The hydrogels were made in the form of circular discs having a uniform diameter of 8 mm and thickness between 4 and 6 mm. The hydrogel discs were compressed up to 60% with a speed of 1% per minute. The compressive modulus was evaluated from the slope of the stress-strain curve (n = 3).

2.7. Preparation of bioink

The immortalized cell line of TVA-BMSCs was established by avian retroviruses possessing SV40 large T Antigen by retroviral expression [22] (gifted by Prof Amitabha Bandyopadhyay, IIT Kanpur). The cells were grown to 80% confluency in Dulbecco's modified Eagle's medium (Gibco) supplemented with 10% fetal bovine serum (Gibco), antibiotic-antimycotic solution 1X (Sigma Aldrich), and 2.5 g/ml. gentamycin (Gibco), referred to as proliferation media. Cell-laden inks were prepared by encapsulating 1 × 10^7 cells/ml to the initially formulated Alg-GG inks and then gently mixed with a spatula.

Table 1
Composition of various inks.

Sample ID	Alg % (w/v)	GG % (w/v)	SNPs (mg/ml, w/v)
Alg-GG-15 N SNP	1	1	15
Alg-GG-30 N SNP	1	1	30
Alg-GG-45 N SNP	1	1	45
Alg-GG-15R SNP	1	1	15
Alg-GG-30R SNP	1	1	30
Alg-GG-45R SNP	1	1	45

Abbreviations: Alg-Alginate, GG-Gellan Gum, N SNPs-Native silk nanoparticles, R SNPs-Regenerated silk nanoparticles.

2.8. 3D CAD model design

The 6-layered 3D construct was designed using the Robocad V 4.0 software (3D Inks LLC, OK, USA) with overall dimensions of 10 mm × 10 mm X 1.5 mm (length x width x height) and an inter-filament length of 2.5 mm in the directions of both x and y axes (Fig. 6A and B).

2.9. Printability assessment

The acellular bioink was loaded into a sterile syringe and secured in the printer's barrel mounted onto a three-axis computer-controlled robotic stage (Fiber Align, Aerotech Inc., Pittsburgh) of Direct Write Assembly [27]. Printing was carried out at 22 °C using a sterile needle (Suzhou Lanbo Needle Co., Ltd, China) with a diameter of 250 μm, at a printing pressure of 7 ± 4 psi, and printing speed of 10 mm/s. Post printing, the constructs were cross-linked with 100 mM of $CaCl_2$ for 30 min under sterile conditions, followed by washing three times with sterile phosphate-buffered saline (PBS).

To determine if the pores correspond to those that were designed, the printability factor (Pr) was determined as [28].

$$Pr = L^2/16A,$$

where A and L represent, respectively, the area and perimeter of the pores in the printed scaffolds. To calculate the printability number, pictures were taken of each scaffold immediately after printing, and image analysis software (ImageJ 2022) was used to measure the perimeter and area of the pores.

2.10. Swelling and degradation study

The printed Alg-GG scaffolds embedded with native and regenerated SNPs and with Silk sol. were immersed in deionized (DI) water at 37 °C for 7 days. The swelling ratio (SR) was calculated using the formula,

$$SR = W_S - W_D / W_D$$

Where W_S corresponds to the weight of the swollen hydrogel at a particular period and W_D represents the dry weight of the hydrogel before immersing in DI water (n = 3).

For *in vitro* degradation assay, the printed constructs were transferred into 6 well plates containing PBS solution at 37 °C. Every two days, a fresh solution was added to the incubation solution. The samples were twice rinsed in distilled water at the predetermined time intervals (day 1, 3, 5, 7, 10) for 10 days (n = 3). The samples' remaining dry masses were then calculated. The original dry weight of each sample at day zero was recorded as W_0, and the remaining dry weight of each sample at day n was marked as Wn [29]. The mass residue ratio was estimated using the following formula:

$$\text{Remaining mass ratio } (\%) = (Wn/W0) * 100$$

2.11. Printing of cell-laden constructs with Alg-GG bioink

As mentioned above, the sterile syringe filled with the bioink was mounted into the bioprinter. Post-printing and crosslinking with 100 mM $CaCl_2$, the scaffolds were transferred to 6 well polystyrene microplates. For the differentiation study, the cells were initially allowed to proliferate in the cell proliferation media for 48 h, then replaced with the chondrogenic differentiation media. The chondrogenic media was composed of DMEM/F12 (Gibco) supplemented with 1X ITS (Sigma-Aldrich), premix (5.33 μg/mL of linoleic acid,1.25 mg of bovine serum albumin) (Sigma-Aldrich), 0.1 μM dexamethasone (Sigma-Aldrich), 37.5 μg/mL ascorbic acid (Sigma-Aldrich), 1 mM sodium pyruvate (Sigma-Aldrich), antibiotic/antimycotic solution 1X (Sigma Aldrich), 2.5 μg/ml. gentamycin (Gibco) and 10 ng/mL TGF-β3 (GeneTex). The 3D bioprinted Alg-GG constructs were examined on days 1, 7, 14, 21, and 28. The media was changed twice every week.

2.12. Gene expression analysis

100 mM EDTA was used to digest the bioprinted constructs containing the native, regenerated SNPs and Silk sol. for 15–30 min at 37 °C to isolate the encapsulated cells. Total RNA was obtained using the RNeasy Mini Kit (Qiagen) according to the manufacturer's protocol. Quantitative RT-PCR was carried out per the protocol in our previous study [22] using the Qiagen primers mentioned in Table 2. GAPDH was used as a housekeeping gene. Cells cultured in a monolayer on day 1 were used as the normalizer. All the reactions were carried out in triplicates.

2.13. Total collagen estimation

Hydroxyproline assay with hydroxyproline as a reference was used to evaluate the total collagen content of the 3D bioprinted constructions on day 14. The experiment was repeated three times (n = 3) [20].

2.14. Immunofluorescence

Constructs on day 28 were collected and fixed with 4% paraformaldehyde for 30 min, followed by rinsing in PBS and permeabilization for 20 min in 0.1% Triton X-100 solution (Millipore Sigma) in PBS. After washing three times for 5 min each with PBS, blocking was done for 1 h in 3% BSA (Bovine Serum Albumin, Sigma-Aldrich) and 0.01% Triton X-100 in PBS [30,31]. The blocking buffer was removed, and samples were incubated overnight at 4° with rabbit anti-collagen II (1:200) (Abcam) and mouse anti-collagen X (1:200) (Abcam) primary antibodies. The next day the solution was rinsed 3 times with 0.3% BSA and 0.01% Triton X-100 in PBS. Secondary antibodies anti-rabbit AlexaFluor 647 and anti-mouse AlexaFluor 488 (both from ThermoFisher Scientific) were incubated in the dark for 2hr at room temperature in PBS (1:200), followed by rinsing with PBS and staining with DAPI (1 mg/mL, 1:300) (Thermo-Fisher Scientific) for 15 min. After final rinsing with PBS, image acquisition was done by Leica SP5 (Leica Microsystems) inverted confocal laser scanning microscope.

2.15. Histological analysis

On day 14, the bioprinted scaffolds from the three sets were collected, washed in PBS, and fixed for 1 h at room temperature in 4% formaldehyde. To analyze cell morphology, 6 μm-thick slices were collected on coated slides and stained with hematoxylin and eosin

Table 2
List of genes analyzed using qRT-PCR.

Gene Name	Full Name	Gene Globe ID	Catalogue No.
GAPDH	Glyceraldehyde-3-phosphate-dehydrogenase	PPH00150F-200	330001
MMP13	Matrix metallopeptidase 13	PPH00121B-200	330001
Col 2A1	Collagen type II alpha 1 chain	PPH02134F-200	330001
Col 10A1	Collagen type X alpha 1 chain	PPH02120E-200	330001
ACAN	Aggrecan	PPH06097E-200	330001
SOX 9	SRY-Box Transcription Factor 9	PPH02125A-200	330001
YAP 1	Yes1 associated transcriptional regulator	PPH13459A-200	330001
TAZ	WW domain containing transcription regulator 1	PPH60066A-200	330001

(H&E) [31].

2.16. Statistical analysis

All data was provided as mean ±SD and investigated using one-way ANOVA followed by Bonferroni's multiple comparison tests with n as the number of different experiments. The differences at $p < 0.05$(*), $p < 0.01$(**), $p < 0.001$(***) and $p < 0.0001$(****) was considered significant. Graph Pad Prism (5.01), San Diego, California, USA, was used for statistical analysis.

3. Results

3.1. Characterization of particles

3.1.1. Zeta potential and DLS

Zeta potential is used to analyze the changes in the surface charge and the electrokinetic property of a colloidal particle under the influence of an applied electric field [32]. The average surface zeta potential for both the native and regenerated SNPs was −21.6 mV and −33.9 mV, respectively (Fig. 1A and B; Table 3). From Table 4, it can be concluded that although the regenerated SNPs showed only moderate stability, they were more stable than the native SNPs, which showed incipient instability [33].

The average size diameter of the SNPs determined by the light scattering particle analyzer was found to be 491.3 d nm for the native, which was much higher than observed for the regenerated SNPs (211.4 d nm) (Fig. 1C and D; Table 3). The polydispersity (pdi) of the SNPs were 0.827 and 1, respectively (Table 3).

3.1.2. FTIR

FTIR was performed to analyze the conformational changes produced during the processing of the SF protein to SNPs (Fig. 2). The absorbance data shows that the peaks at 1623 cm^{-1} and 1514 cm^{-1} confirm the presence of the β-sheet structure in SNPs. The FTIR absorbance plot for native and regenerated SNPs illustrates the presence of the same peaks. This indicates no adverse structural changes in the SNPs. We performed deconvolution for the amide I region ranging from 1590 to 1705 cm^{-1} to determine the makeup of the secondary structure in the SNPs [35,36] (Fig. 2C and D). The β-sheet peak at 1632 cm^{-1} present in native SNP moved to 1625 cm^{-1} in the regenerated SNP. This indicates a higher molecular weight of β-sheet in the native SNP. Whereas the α-helices in both regenerated and native SNP remained unmoved. The peak for β-turn shifted from 1696 cm^{-1} in the native SNP to 1694 cm^{-1} in the regenerated counterpart. The total β-crystals present in native SNP was 74%, which decreased in regenerated SNP during processing to 68%. At the same time, the random coil content was increased from 10% to 29% on dissolution and reconstitution(Fig. 2B); as-spun silk protein is present in the silk I structural conformation which has maximum β content present [37].

Table 3
Zeta Potential, polydispersity index (pdi) and average size of SNPs.

SNPs	Zeta Potential (mV)	Polydispersity Index (pdi)	Average Size (d. nm)
Native	-21.6	0.827	491.3
Regenerated	-33.9	1.000	211.4

Table 4
[34]Colloidal stability behavior for a range of distinct zeta potential (ASTM Standard D 4187-82, 1985)distinct zeta potential (ASTM

Zeta Potential (mV)	Stability behavior of the colloid
From 0 to ± 5,	Rapid coagulation or flocculation
From ±10 to ±30	Incipient instability
From ±30 to ±40	Moderate stability
From ±40 to ±60	Good stability
more than ±61	Excellent stability

3.2. Rheological characterization

The process for forming Alg-GG hydrogel by adding SNPs is illustrated in Fig. S1.

3.2.1. Flow behavior

The flow behavior of all the samples was investigated at 25 °C and correlated with the generated shear rate (193.7–386.7 s^{-1}) on the 250 μm micronozzle during 3D bioprinting. Fig. 3A shows that only Alg hydrogel displayed a Newtonian behavior, whereas only GG showed a shear thinning behavior. The addition of Silk sol. to the already prepared 1:1 ratio Alg-GG hydrogel did not influence the flow property of the

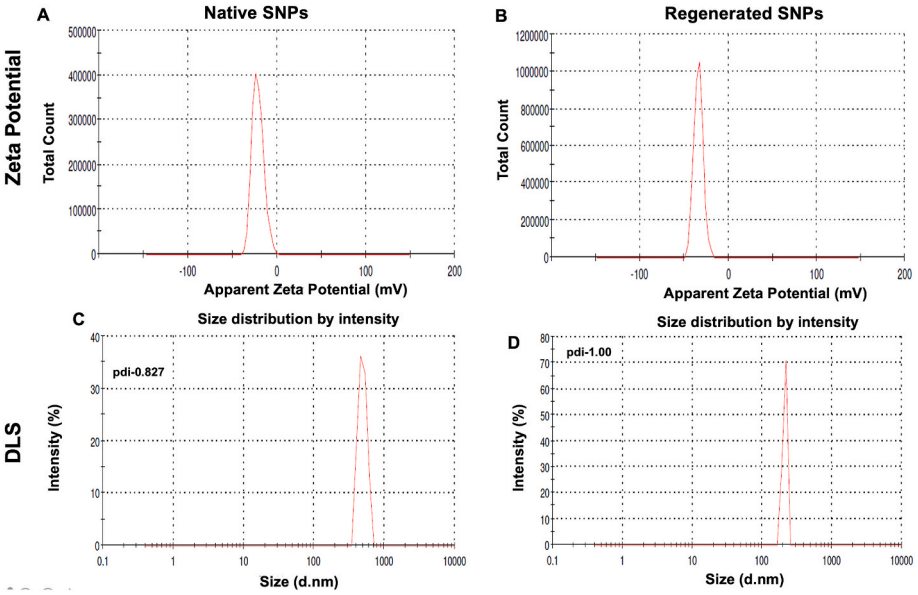

Fig. 1. (A and B) Graph of Zeta potential analysis of Native and Regenerated SNPs respectively **(C and D)** Graph of the particle size distribution (DLS) of Native and Regenerated SNPs, respectively.

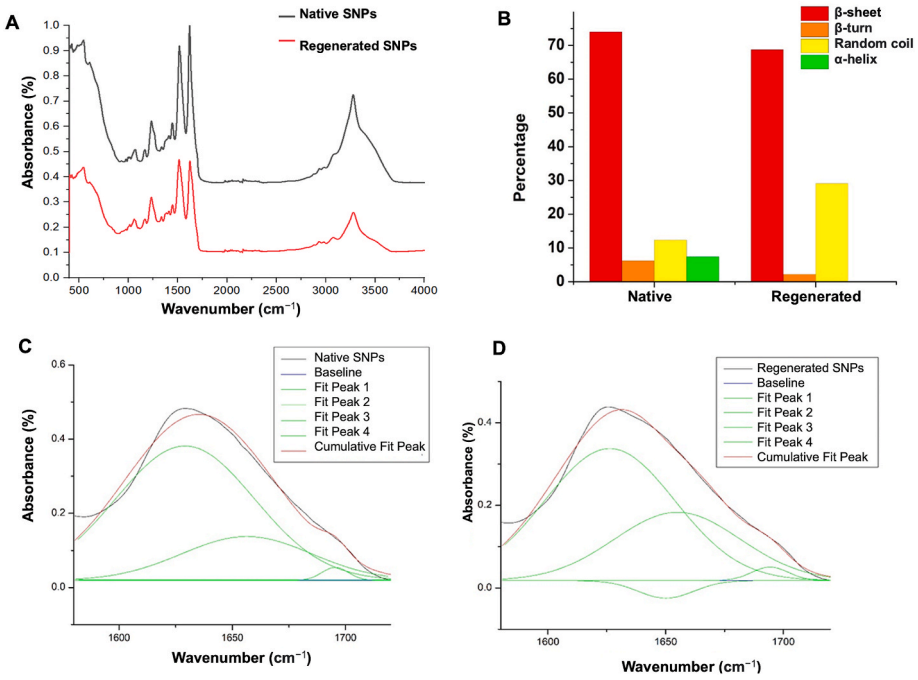

Fig. 2. **(A)** FTIR spectra of Native and Regenerative SNPs **(B)** Percentage secondary conformation in Amide I region **(C)** FSD spectra of Native SNPs in Amide I region **(D)**FSD spectra of Regenerated SNPs in Amide I region.

blend as both the Alg-GG-Silk sol. and Alg-GG groups demonstrated a similar shear thinning behavior with an approximately 2-fold decrease in shear viscosities. It is to be noted that the incorporation of SNPs (both native and regenerated) to the Alg-GG hydrogel depicted an increase in initial viscosities of the blend **(Table 5)** with multifold viscosity drops (Fig. 3B and C) when the respective hydrogels were subjected to a shear rate of 200 s^{-1} and 400 s^{-1}. Although displaying a shear-thinning behavior, both Alg-GG-45 N SNP and Alg-GG-45R SNP exhibited extremely high viscosities making it challenging to mix cells for 3D bioprinting. Hence, these groups were not considered for further experiments.

The shear-thinning nature of different combinations of Alg and GG hydrogels with different SNPs and Silk sol. was quantified using the Power law equation,

$$\eta = K\gamma n^{-1} \ldots \ldots \quad \text{Eq.1}$$

where K is the consistency index, n is the shear-thinning coefficient, γ represents shear rate, and η corresponds to apparent viscosity. From Table 6, it is clear that all different combinations of Alg-GG hydrogels with three different combinations of native and regenerated SNPs (15, 30, and 45 mg/ml) exhibited a shear thinning behavior ($n < 1$).

The yield stress was calculated from the shear stress vs. viscosity graph, which determines the minimum pressure necessary for the polymer solution to flow. It was observed from Fig. 4A that the yield stress value increased from 0.3784 kPa in the Alg-GG-Silk sol. group to 0.48574 kPa in the Alg-GG-15 N SNP group. Thus, the SNP played a significant role in altering the rheological properties of Alg-GG hydrogel.

3.2.2. *Oscillatory amplitude and frequency sweep*

The storage modulus (G') of Alg-GG hydrogel evaluated from the amplitude sweep experiment slightly increased from 2.493 Pa to 5.09 Pa (2-fold) with storage modulus (G') > loss modulus (G″) post addition of Silk sol. to the blend as observed from Fig. 3D. Incorporating native and regenerated SNPs into the Alg-GG hydrogel blend also resulted in increased storage modulus that depicted an increasing trend with increasing SNP concentration (Fig. 3E and F). The position (strain %) of occurrence of flow point for both the native and regenerated group increased with increasing concentration of the incorporated SNPs with further later occurrence in case of the regenerated sample group. A strain of 2% was used for further frequency sweep analysis to avoid sample breakdown during the experiment. From all the graphs (Fig. 3G, H, I), a dependent relationship between both storage (G') and loss modulus (G″) with the angular frequency (ω) was observed with both G' and G″ running almost parallel to each other for the entire range. This dependency of G' and G″ with ω is more prominent for native SNP embedded hydrogels than regenerated counterparts for all concentrations. The loss factor or tan δ value plays a pivotal role in determining the printability of a hydrogel. A loss factor value between 0.4 and 0.6 is ideal for 3D bioprinting [38]. Fig. 4C shows that Alg-GG hydrogels containing native and regenerated SNPs demonstrated a loss factor value of 0.454 and 0.381, respectively, compared to 0.078 in control (Alg-GG-Silk sol.) at a 100 rad s^{-1} angular frequency.

However, considering the critical parameters for 3D bioprinting (shear thinning behavior (n), shape fidelity post-printing (η)) and subsequent mechanical property (storage modulus) for structural stability and articular cartilage differentiation, we have chosen 15 mg/ml of regenerated and native SNPs for further experimental procedures.

3.2.3. *Shear recovery*

The shear recovery test was performed to assess the gel recovery property of the hydrogel post exhibiting shear thinning behavior. The experiment was carried out for three different shear rates (0.001 s^{-1}, 200 s^{-1}, and 0.001 s^{-1}), replicating the shear rates applied on the hydrogel during the other timeline of 3D bioprinting (pre-extrusion, extrusion, and post extrusion). A 77.60% shear recovery was achieved in the case of Silk sol. incorporated Alg-GG hydrogel, which increased to 78.69% and 80.36% for Alg-GG-N SNP and Alg-GG-R SNP groups, respectively (Fig. 4B). Thus, the addition of SNPs in the Alg-GG blend enhanced the gel recovery characteristic of the composite hydrogel, an essential requirement for achieving post-printing structural stability.

The overall values of Yield stress, loss factor, and percentage recovery of the various hydrogel blends are mentioned in Table 7.

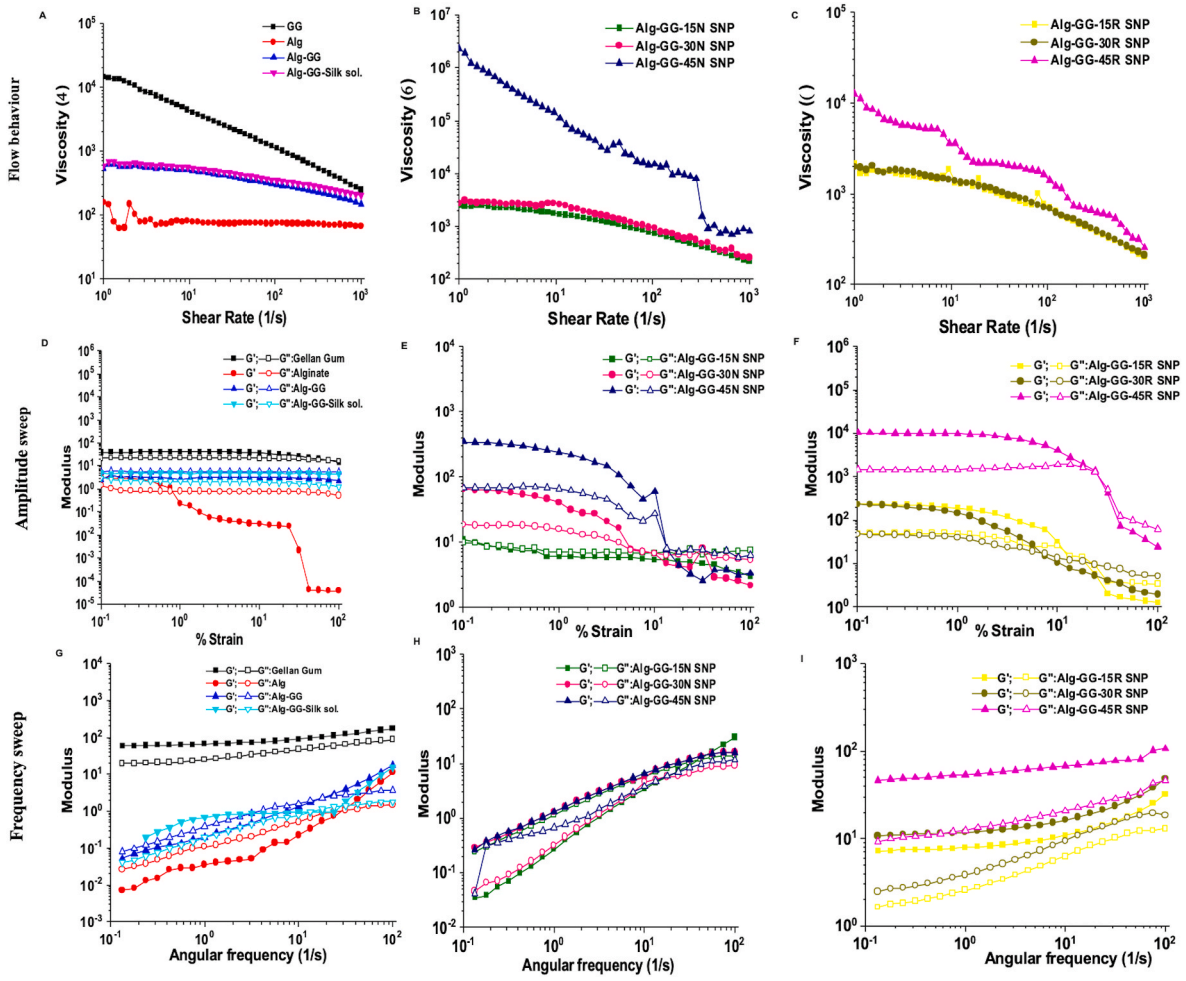

Fig. 3. Flow behavior of **(A)** GG, Alg, Alg-GG, Alg-GG-Silk sol. **(B)** Alg-GG-15 N SNP, Alg-GG-30 N SNP, Alg-GG-45 N SNP **(C)** Alg-GG-15R SNP, Alg-GG-30R SNP, Alg-GG-45R SNP Amplitude Sweep of **(D)** GG, Alg, Alg-GG, Alg-GG-Silk sol. **(E)** Alg-GG-15 N SNP, Alg-GG-30 N SNP, Alg-GG-45 N SNP **(F)** Alg-GG-15R SNP, Alg-GG-30R SNP, Alg-GG-45R SNP Frequency Sweep of **(G)** GG, Alg, Alg-GG, Alg-GG-Silk sol. **(H)** Alg-GG-15 N SNP, Alg-GG-30 N SNP, Alg-GG-45 N SNP **(I)** Alg-GG-15R SNP, Alg-GG-30R SNP, Alg-GG-45R SNP.

Table 5
Shear viscosities of different standalone and composite hydrogels at 3D bioprinting shear rates.

Sample ID	1 s^{-1}	200 s^{-1}	400 s^{-1}
GG	14802	709.99	446.57
Alg	156.64	72.95	69.955
Alg-GG	543.73	256.59	209.26
Alg-GG-Silk sol.	593.73	306.59	259.26
Alg-GG-15 N SNP	2528.7	518.88	350.39
Alg-GG-30 N SNP	2730.7	585.02	391.87
Alg-GG-45 N SNP	2363000	9536.2	1036.5
Alg-GG-15R SNP	2154.3	458.58	326.33
Alg-GG-30R SNP	1950.7	474.74	333.87
Alg-GG-45R SNP	12588	723.49	576.17

3.3. Mechanical testing

The tensile testing was carried out to determine the stretchability of the formulated hydrogel combinations. The tensile modulus (Fig. 5D) calculated from the stress-strain curve (Fig. 5A) was observed to be higher (26.8 kPa) in the case of native SNPs embedded in Alg-GG hydrogel as compared to its regenerated counterpart (4.46 kPa) and Alg-GG-Silk sol. control group (18.9 kPa). A similar trend was also observed for tensile strength (817.85 kPa for Alg-GG-N SNP, 382.9 kPa for Alg-GG-Silk sol., and 104.4 kPa for Alg-GG-R SNP) determined at the fracture point (**Table 8**). The stress-strain graph of the hydrogels (Fig. 5B) and force-displacement curve (Fig. 5C) obtained from compression testing demonstrated a J-shaped curve with an initial toe region. The compressive modulus determined from the slope of the graph(Fig. 5E) was in the range of 317.2 kPa for the Alg-GG-Silk sol. group, 187.25 kPa for Alg-GG-N SNP, and 257.65 kPa for Alg-GG-R SNP similar to the range of determined compressive modulus of native articular cartilage (240–1000 kPa) [39].

3.4. Printability of the multicomponent bioink

By employing the printability value (Pr) of the pores and taking into account the printing resolution in 3D of the bioprinted constructs, the printability of the SNP reinforced bioinks and the influence of the post-crosslinking were evaluated. The image of the printed scaffold post

Table 6
Quantification of shear-thinning behavior of Silk solution and SNPs incorporated Alg - GG hydrogel.

Sample ID	Power law equation	R^2 value of equation	K = consistency index (Pa s^n)	n = power law index (dimensionless)
Alg-GG-Silk sol.	$\eta = 657.17\gamma^{-0.283}$	0.9953	657.17	0.717
Alg-GG-15 N SNP	$\eta = 3682\gamma^{-0.652}$	0.9748	3682	0.348
Alg-GG-30 N SNP	$\eta = 4229.9\gamma^{-0.682}$	0.951	4229.9	0.318
Alg-GG-45 N SNP	$\eta = 3 \times 10^6\gamma^{-0.74}$	0.8711	3×10^6	0.26
Alg-GG-15R SNP	$\eta = 1884.4\gamma^{-0.544}$	0.9534	1884.4	0.456
Alg-GG-30R SNP	$\eta = 1989.4\gamma^{-0.556}$	0.9788	1989.4	0.434
Alg-GG-45R SNP	$\eta = 13393\gamma^{-0.36}$	0.9367	13393	0.64

crosslinking is shown in Fig. 6C, D, and E. The range of pressure varied with different bioinks due to the viscosity variation. The pressure needed for the control ink was 3.5 ± 1.5 psi; 5 ± 2 psi, and 7 ± 3 psi for the bioink with the native and regenerated SNPs. The pore structure imaged for determining the Pr value is depicted in Fig. 6G, H, I. The mean Pr values were 0.84913878, 1.00036814, and 0.89781258 for the control, bioink with the native, and regenerated, respectively (Figure 6L). The mean area and perimeter of the pores of the bioprinted constructs for the three groups are shown in Fig. 6J and K. The relative standard deviations were used to assess the 3D construct's printing consistency and showed consistency across all the printed compositions.

3.5. *Swelling and In vitro degradation behavior*

All the three sample groups (Alg-GG-Silk sol., Alg-GG-15 N, and Alg-GG-15R) demonstrated an increased swelling ratio with an increasing period. A spike in the swelling ratio has been observed from day 1 to day 5 for all the hydrogel blends, i.e., from 0.097 ± 0.009 to 0.4305 ±

Table 7
Yield stress, loss factor, and percentage recovery of Alg-GG-Silk sol., Alg-GG-15 N SNP, and Alg-GG-15R SNP hydrogel blends.

Sample ID	Yield stress (Pa)	Loss factor	% Recovery
Alg-GG-Silk sol.	0.3784	0.078	77.60
Alg-GG-15 N SNP	0.48574	0.454	80.36
Alg-GG-15R SNP	0.1736	0.381	78.69

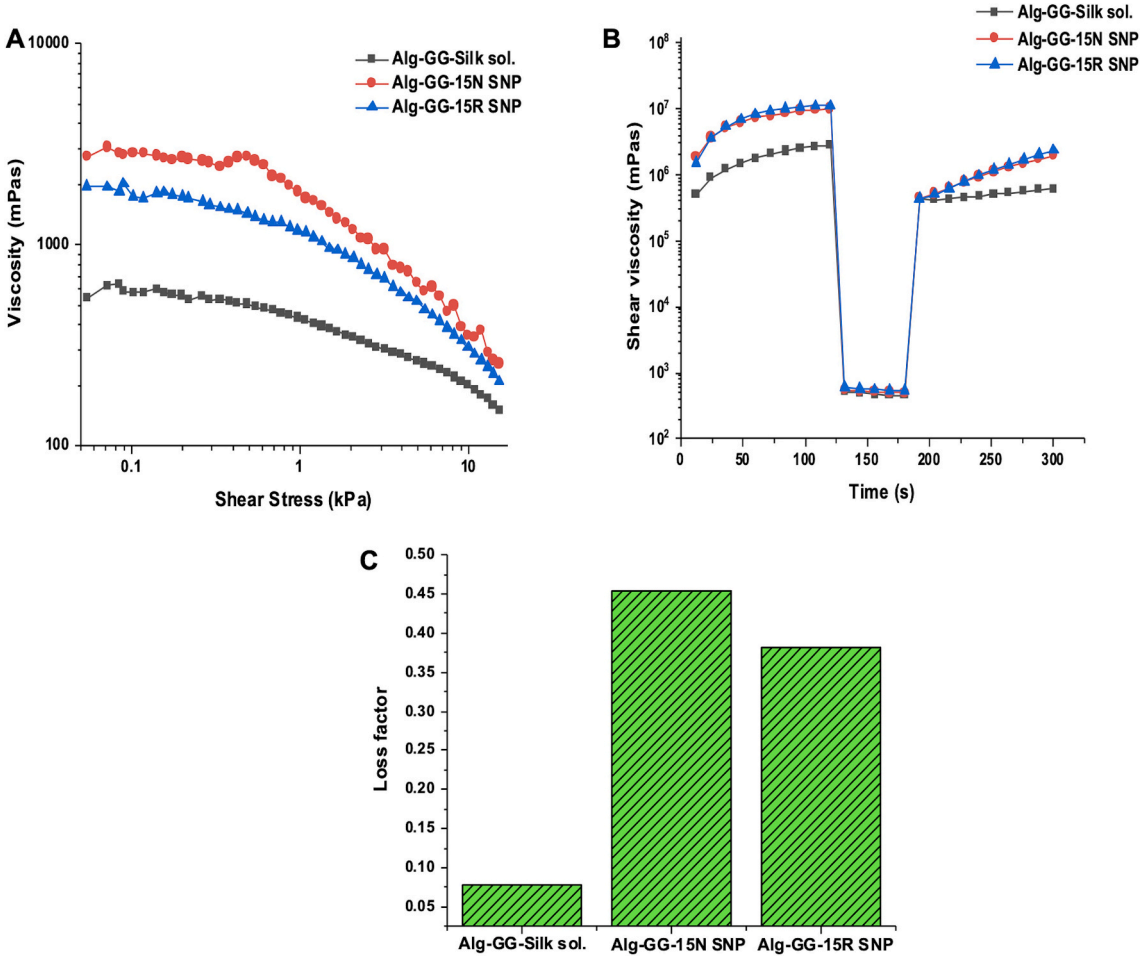

Fig. 4. **(A)** Viscosity vs. shear stress plot to determine the yield stress of the hydrogel blends (Alg-GG-Silk sol., Alg-GG-15 N SNP, Alg-GG-15R SNP) **(B)**Shear recovery analysis of the chosen hydrogel blends **(C)** The loss factor values determined from frequency sweep analysis.

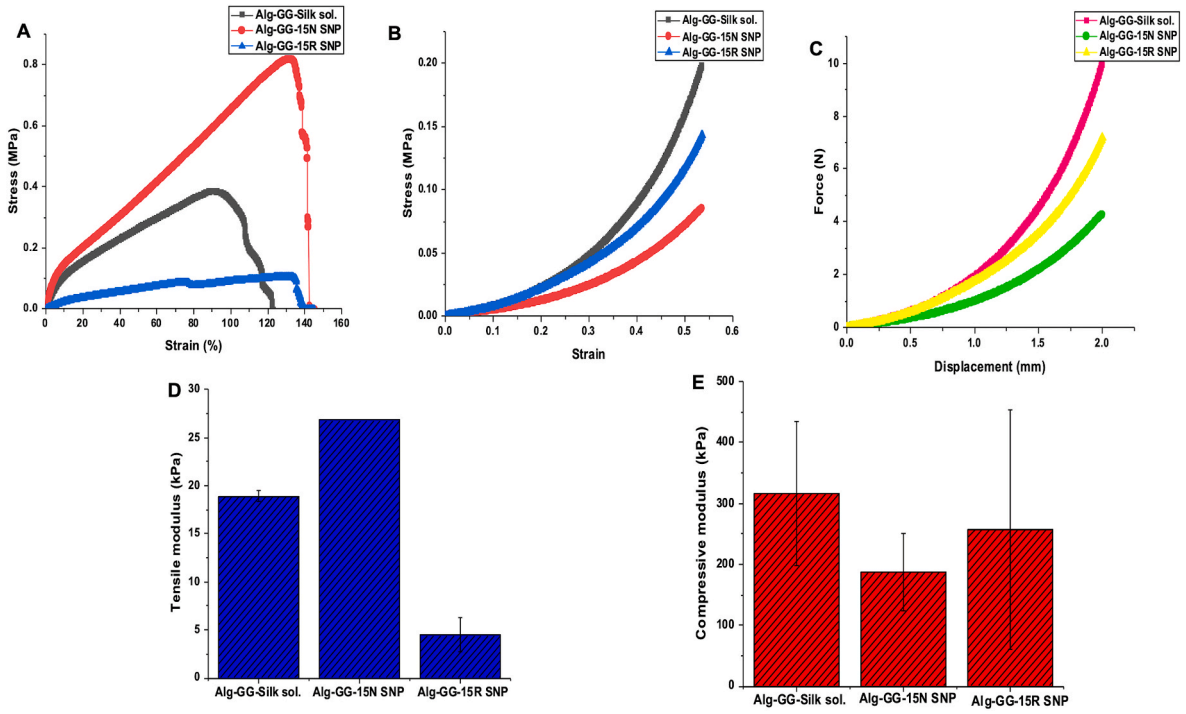

Fig. 5. **(A)**Stress-strain curve for tensile testing of Alg-GG films incorporated with Silk sol. and SNPs (native and regenerated) **(B)** Stress-strain curve and **(C)** Force-displacement curve for compression testing of Alg-GG hydrogel discs incorporated with Silk sol. and SNPs (native and regenerated) **(D)** Determination of tensile modulus from the slope of the stress-stain curve **(E)** Determination of compressive modulus from the slope of the stress-strain plot.

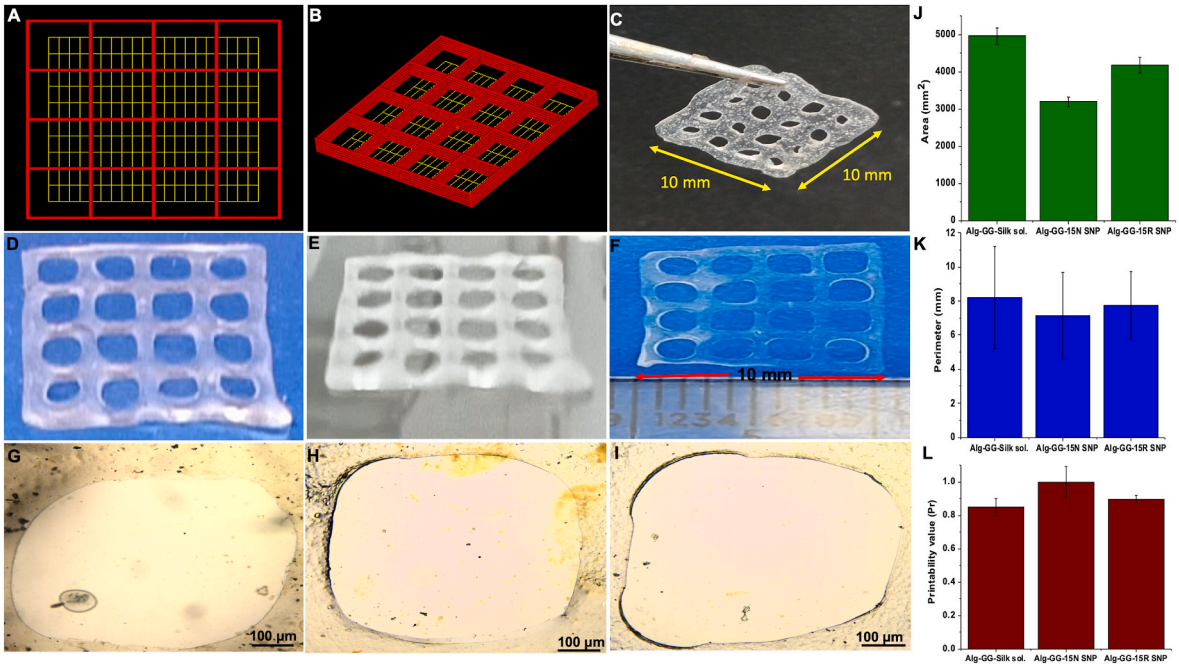

Fig. 6. **(A)** Top view of the designed CAD model (B)Isometric view of the CAD model (C) Representative image of the 3D bioprinted scaffold (D) Top view and (E) Side view of the bioprinted scaffold (F) Scale measurement post-printing elucidating 10 × 10 mm printed construct (G, H, I) Microscopic image of the pores of the 3D printed scaffold, i.e., Alg-GG-Silk sol., Alg-GG-15 N SNP, Alg-GG-15R SNP (J, K, L) Area, perimeter and printability value(Pr) of the pores of the three groups of the printed scaffold.

0.0148 in the case of Silk sol. group, from 0.08 ± 0.005 to 0.483 ± 0.133 in case of native SNP group, and from 0.100 ± 0.0122 to 0.383 ± 0.028 in case of regenerated sample group (Fig. 7A).

The *in vitro* degradation kinetics demonstrated that bioink with the native SNPs showed a constant decline in the % mass starting from day 1; at the end of day 10 the remaining mass % was found to be 83.61 ± 0.47. Whereas for the control and the bioink with the regenerated SNP, the values were 91.98 ± 1.25 and 87.25 ± 0.47%, respectively (Fig. 7B).

Table 8
Mechanical properties of Alg-GG-Silk sol., Alg-GG-15 N SNP, and Alg-GG-15R SNP hydrogel blends.

Sample ID	Tensile strength (kPa)	Tensile modulus (kPa)	Compressive modulus (kPa)
Alg-GG-Silk sol.	382.9	18.9	317.2
Alg-GG-15 N SNP	817.85	26.8	187.25
Alg-GG-15R SNP	104.4	4.46	257.65

3.6. Gene expression analysis

We assessed the chondrogenic differentiation ability of the TVA-BMSCs encapsulated in the Alg-GG bioprinted constructs using the specific differentiation markers mentioned in Table 2 on 1, 7,14,21,28 days of culture normalized using GAPDH. All the three sets of the bioprinted construct that is Alg-GG with native, regenerated SNPs and Silk sol. exhibited an increase in the expression with the chondrogenic markers, i.e., ACAN, COL 2A1, and SOX 9 from day 1 to day 28 (Fig. 8). However, enhanced expression was mainly obtained with the Silk sol. set at time points compared to its other counterpart. Infact a significant fold change of around 9 was obtained on day 28 with ACAN, whereas half of its expression (4.5) was observed with the regenerated SNP part. A similar trend was observed with COL 2A1 (fold change 9) and SOX 9 (fold change 5.2) compared to the native and regenerated SNP. Around 3- and 2-times enhanced expression of SOX 9 at day 28 for the Silk sol. was obtained compared to the regenerated and native SNPs, respectively. Contrasting results were obtained with the hypertrophy markers COL 10 and MMP 13. A decline in the expression level of COL 10 from day 1 to day 28 was observed in the Silk sol. set, also observed with the native SNP part. However, on day 7 there was a sudden rise in the expression level with the regenerated SNP, where the declining trend continued till day 28.

Interestingly, the expression level in the case of the Silk sol. was significantly less than in the other two sets. In the case of MMP 13 although no significant difference in expression levels was observed till day 14, a sudden decline in the expression level (around one-fold) was conspicuous on day 21 for the Silk sol. constructs that continued till day

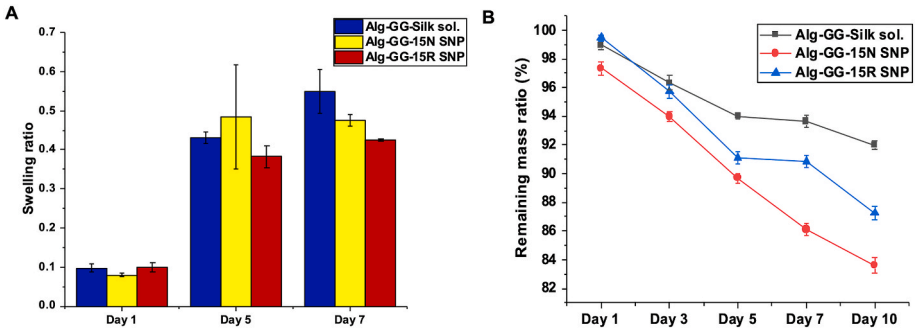

Fig. 7. Swelling and degradation analysis graphs over 7 days and 10 days, respectively.

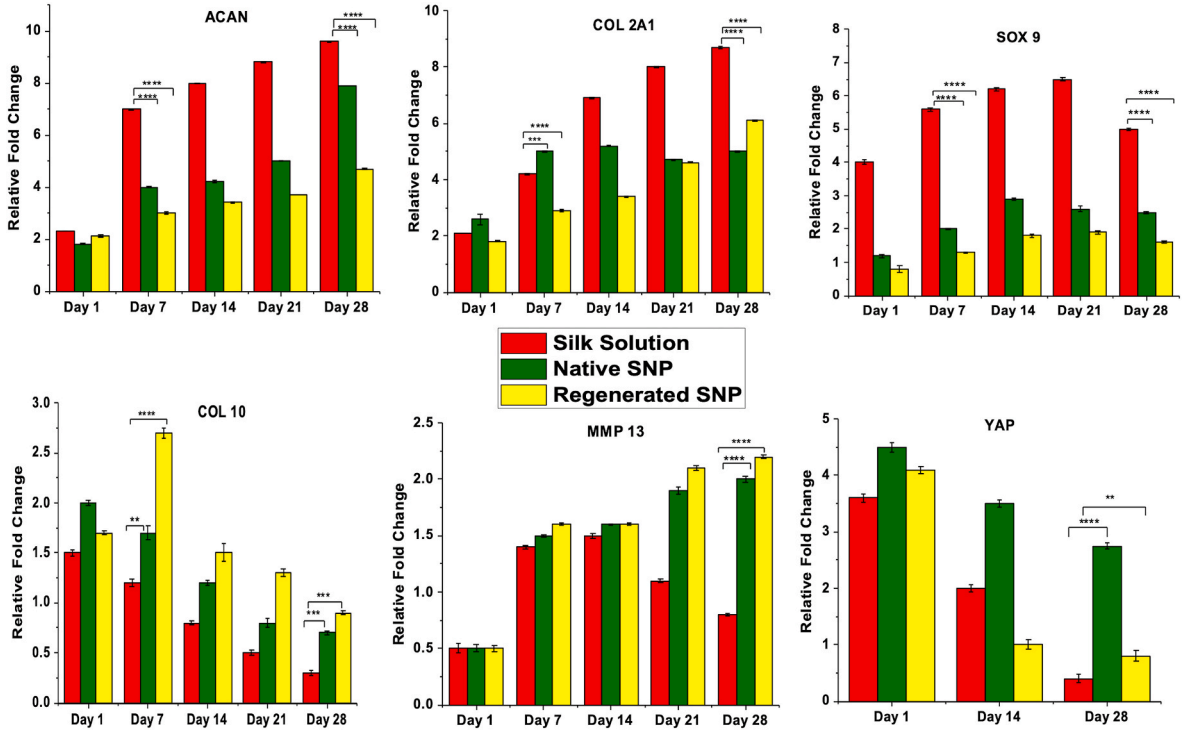

Fig. 8. Comparative gene expression analysis for TVA-BMSCs laden Alg-GG bioprinted constructs containing Native SNPs, Regenerated SNPs and Silk sol. for the set of chondrogenic differentiation-specific genes, significant at $p < 0.05$(*), $p < 0.01$(**), $p < 0.001$(***) and $p < 0.0001$(****).

28. YAP gene, a negative regulator of chondrogenesis, was found to have the least expression with the Silk sol. set, which exhibited a decline in expression from day 1 to day 28. At the same time, a substantial difference in the expression of the native and regenerated SNP was found with respect to the Silk sol. counterpart. We also assessed the TAZ gene; however, no expression was found.

3.7. Total collagen estimation

A hydroxyproline assay was carried out to determine the total collagen content (Fig. 9) on day 14 in the bioprinted constructs. The results obtained validated our gene expression findings. Minimum collagen production of 0.075 μg/mg was observed in the bioprinted construct with regenerated SNPs, which showed a significant result ($p < 0.0001$) compared to the control Silk sol. In the case of constructs with native SNPs, the collagen content was also significant at ($p < 0.0001$), i.e., 0.14 μg/mg compared to the Silk sol. set. The bioprinted construct with Silk sol. exhibited the highest amount of collagen, which was found to be 0.285 μg/mg [40].

3.8. Immunofluorescence analysis

In order to envisage the collagen II (chondrogenic differentiation marker) and collagen X (hypertrophic marker) protein production, immunofluorescence analysis was carried out on day 28 for all three sets of samples. Noticeable collagen II expression was observed in all three sets of the bioprinted construct; however, the expression in the Alg-GG with the Silk sol. was found to a greater extent than the SNP counterparts (Fig. 10), which validates the findings of the gene expression. On the other hand, the discrete expression of collagen X was observed in the cytoplasm of all the three sets of the bioprinted construct, especially with the construct with Silk sol. (Fig. 11).

3.9. H&E

H&E was performed to determine the temporal changes in cellular morphology, the cellular distribution of the encapsulated TVA-BMSc in the bioprinted construct, and chondrogenesis. From the staining images, it was evident that there was a uniform distribution of the cells in all three sets of the bioprinted constructs; however, higher cellular density in the Alg-GG construct with Silk sol. was conspicuous (Fig. 12A and B). Although the cells in the scaffold with Silk sol. seemed to have a slight change, as evident in 100X, cells in both types of SNPs were distinct with large nuclei. Even pericellular lacunae were also apparent in the bioprinted construct with the SNPs (Fig. 12 G, H, and 7 K, L). In the Silk sol. set, although the lacunae were found to be restricted compared to their SNPs counterparts, however, it must be noted that the cells were found to have migrated towards the pores and have resulted in the formation of cytoplasm over 14 days (shown by arrow) (Fig. 12C and D). ECM formation was also conspicuous in this set of the bioprinted construct. The encapsulated MSCs in the bioprinted constructions had a spherical form, a favorable configuration for chondrocytes. Maintaining this morphology on day 14 during culture indicates cell-cell and cell-matrix interaction and suggests that the metabolism is triggered by ECM formation around the cells.

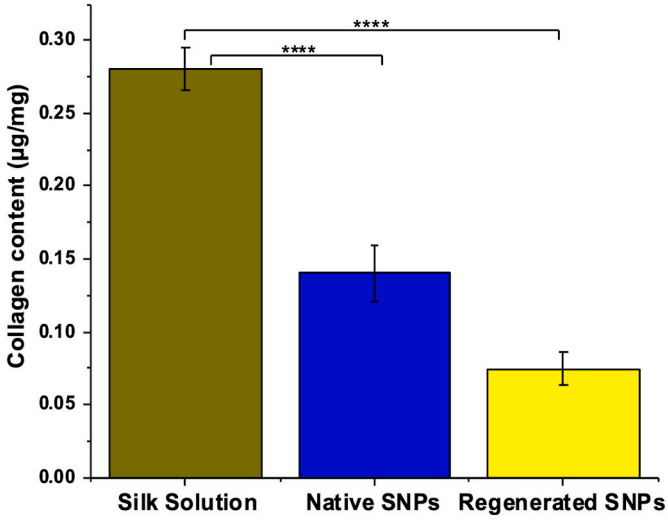

Fig. 9. Biochemical estimation of the total collagen content in the 3D bioprinted constructs, significant at $p < 0.0001$(****).

4. Discussion

This study reports the utilization of a newly developed bioink composite. The polymers used in generating this multicomponent bioink are already established for medical use. For example, Alg has been used extensively in therapeutic settings for decades, primarily for wound healing and drug administration [8,41], whereas GG has been employed mainly for drug delivery [42]. The unique feature of this study was the use of SNPs as reinforcement to improve the printability of the bioink, apart from ameliorating the shape fidelity.

The difference in potential between the dispersion medium and the stationary layer of fluid connected to the dispersed particle is the zeta potential [43]. The charge on the SNPs affects their physicochemical properties, which are crucial in their interplay with the cells [44]. The surface charge on the SNP can result in an elevated absolute value of zeta potential. In particular, NPs are described as stable at an absolute zeta potential value of more than 30 mV [45]; hence from Table 4 it can be concluded that the regenerated SNPs synthesized would persist in a stable colloidal state. The less stability of the native SNP may result in their aggregation due to the Van der Waals attractive forces [46]. It means that the suspension of SNPs becomes more stable on the fabrication of the regenerated SNPs. Since the pH of the solution was maintained at 7 in both the SNPs, variation in zeta potential due to pH was not observed. The higher average size diameter of the native SNP indicates a slight aggregation of the particles [47]. PDI values greater than 0.7 specify that the sample holds a very broad particle size distribution [48]. Negatively charged SF particles enable the interaction of the NPs and the positively charged cells, which is helpful for *in vivo* or *in vitro* studies [49]. This preferential binding can be attributed to the suitable electrostatic interactions [50]. As the SF polypeptide chains are arranged in definite β-sheets conformation, which is stabilized by inter and intramolecular hydrogen bonds, hence, to dissolve the SF, the bridging bonds are disrupted. This might be one of the probable reasons for the smaller size of the regenerated SNP compared to the native ones [51]. While processing the SF, gelation of the Silk sol. may happen due to the aggregation of abundant GAGAGS sequences in Silk chains. The SNPs formed using cryomilling, which involved a high-stress application, inducing β-crystallization, as depicted in the FTIR result.

Much research has concentrated on 3D printing inks consisting of micro or nanoparticle [52]. However, the spherical particle's local flow differs from the non-spherical ones, which might influence the suspension viscosity [53]. As a result, various rheological tests were used to determine the impact of particle size and proportion on the ink's behavior. Investigating the shear-thinning behavior of the hydrogel is a prerequisite for extrusion-based 3D bioprinting to ensure smooth extrusion and higher cell viability post extrusion [54]. The flow behavior analysis (shear rate weep) revealed a decrease in shear viscosity at the bioprinting shear rates for all the standalone and composite hydrogels except Alg, which displayed a Newtonian behavior. At the bioprinting shear rates (200 and 400 s-1), Silk sol. added Alg-GG hydrogel illustrated a similar viscosity drop as the Alg-GG hydrogel with similar initial viscosities revealing the negligible role of Silk sol. in modulating the flow property of the Alg-GG hydrogel. However, both

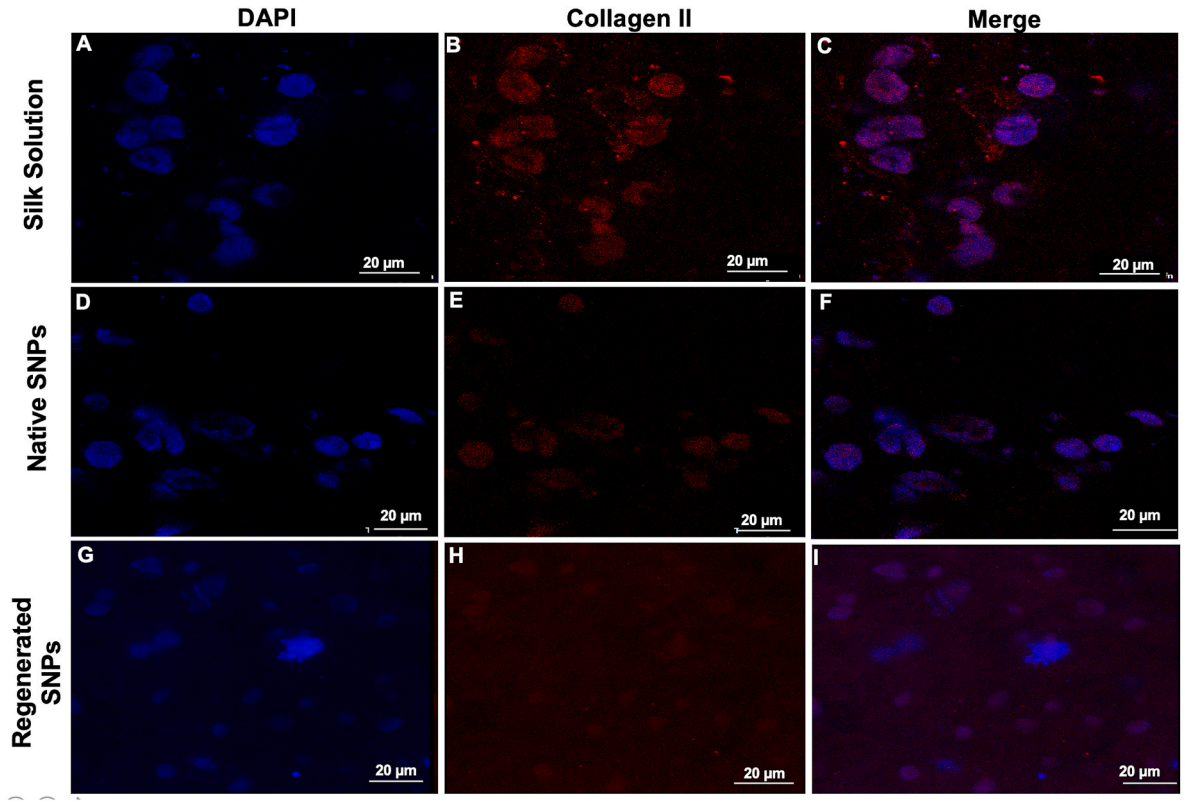

Fig. 10. Immunofluorescence analysis depicting the protein expression of Collagen II in three different Alg-GG bioprinted constructs with Native SNPs, Regenerated SNPs, and Silk sol.

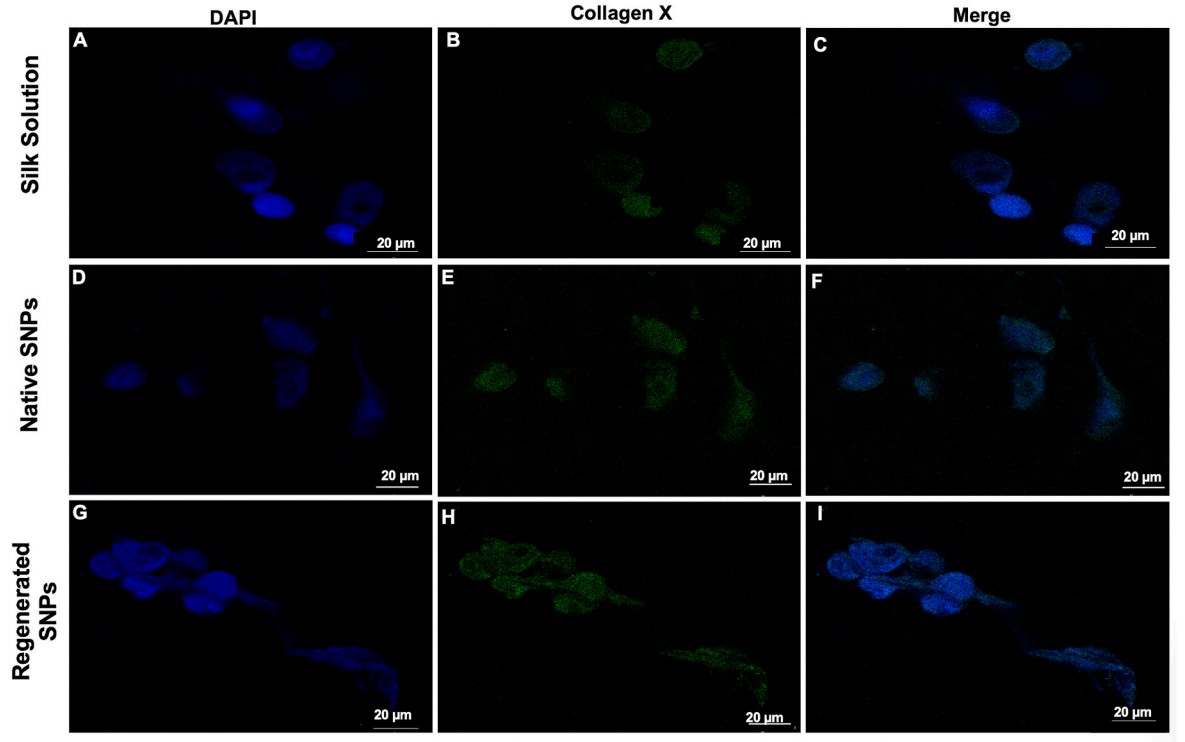

Fig. 11. Immunofluorescence analysis depicting the protein expression of Collagen X in three different Alg-GG bioprinted constructs with Native SNPs, Regenerated SNPs, and Silk sol.

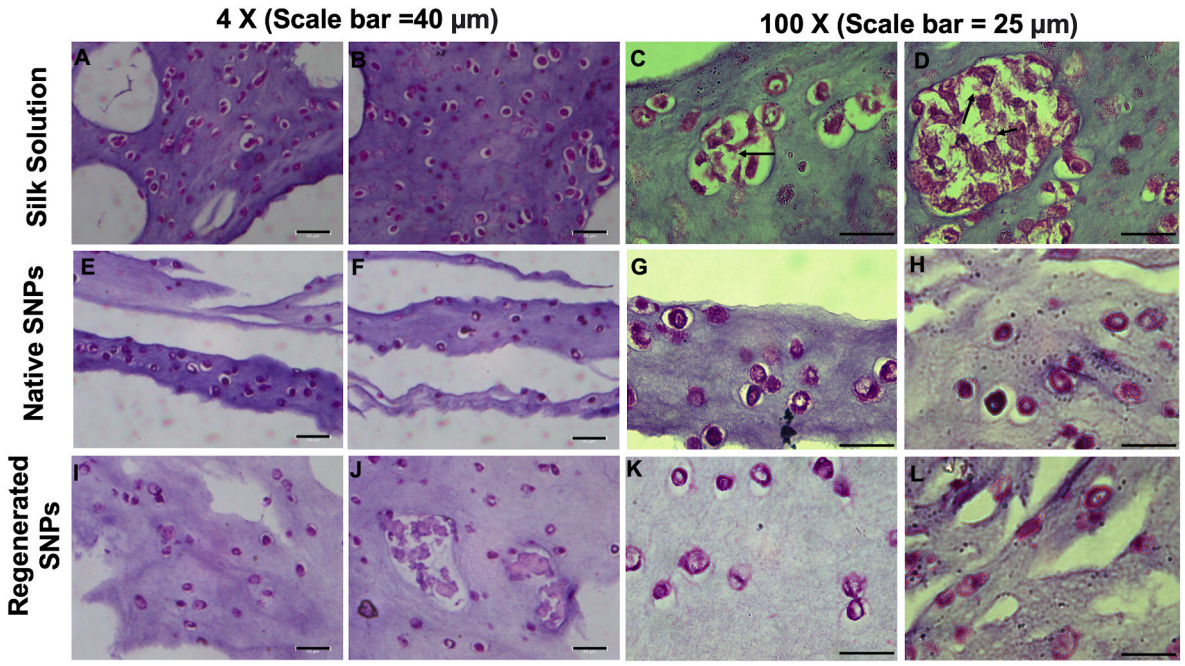

Fig. 12. H&E Images of the bioprinted constructs on day 14 containing **(A–D)** Silk sol., **(E–H)** Native SNPs, **(I–L)** Regenerated SNPs.

the native and regenerated SNP incorporated Alg-GG hydrogels exhibited an increase in initial shear viscosity and a corresponding drop in viscosity (Table 5) at the desired bioprinting shear rates for all the concentrations as compared to the Alg-GG and control group. This remarkable difference was further confirmed by the shear-thinning coefficient evaluation, where the nanocomposite hydrogels illustrated a better shear-thinning coefficient value than the Silk sol. control group. The viscoelastic characteristic of any hydrogel (determined using amplitude and frequency sweep) plays a crucial role in determining the structural stability of the 3D bioprinted construct. The oscillatory amplitude and frequency sweep analysiss revealed an increase in storage modulus (G') in all the nanocomposite hydrogels (both native and regenerated) with increasing SNP concentration with a strong dependence of both modulus on the angular frequency (ω). Such dependency corresponds to the formation of relatively weak gel system as described by Marapureddy et al. [55]. The enhancement of hydrogel's mechanical stability (G') and shear thinning property with the inclusion of NPs is assumed due to the reversible electrostatic interactions of the NPs. This phenomenon of enhanced rheological characteristics with the incorporation of NPs in the hydrogel in a broad spectrum has been extensively reviewed by Chakraborty et al. [56].

The inclusion of the NPs in the polymeric mixture resulted in a remarkable mechanical improvement in the shear-thinning, G′, which may be allocated to the reversible and the electrostatic cross-linking of the NPs. Similar results were obtained by Kesti et al. [13] and Lee et al. [14], where they reported a remarkable improvement in the shear-thinning property, G′, along with the mechanical strength post-cross-linking obtained upon the inclusion of the cartilage ECM particles and cationic NPs respectively. Lesser G′ was obtained with Alg of lower molecular weight than Alg with higher molecular weight. Interestingly, the G′ value improved when aminopropyl-modified aminated cationic Si NPs were added[14]. However, it should be noted that in our study, the molecular weight of Alg was kept constant; as a result, enhanced G′ values were obtained when SNPs were added to the bioink component. The yield stress value signifies the shear stress at which the polymer starts to flow. In our experimental analysis (Fig. 4A), the control group demonstrated yield stress of 0.3784 kPa, which increased to 0.48574 kPa (1.28-fold) upon adding 15 mg/ml native SNPs to the hydrogel blend. An interesting observation from Fig. 4A is the low yield stress for the regenerated group (0.1736 kPa) which can be attributed to the degradation of the SF protein during the regeneration process that might have influenced the polymer-NP interaction [57]. An 80% viscosity recovery is considered suitable for forming structurally stable multilayer constructs [58]. We evaluated the thixotropic nature of the composite hydrogels through three different bioprinting timelines: 0.001s-1 to represent the zero-shear viscosity of the sample, 200 s-1 to represent the breakdown of the polymeric entanglements due to shear rate at the tip of the nozzle and again a low shear interval of 0.001s–1 to regain the structural stability. An approximate 80% recovery have been observed for all the sample groups (with and without SNP) ensuring good shape fidelity post-printing.

The knee joint of our body supports the maximum load in terms of compression, stretching, and flexion, balanced by the articular cartilage. Thus, the hydrogel's mechanical property directly impacts the development of articular cartilage due to its inherent property of mechanical loading *in vivo*. Our study focused on evaluating SNPs incorporations' role in influencing the Alg-GG hydrogel's mechanical properties. From Fig. 5, variability in the trend of the tensile and compression modulus of the hydrogel blends by *Drozdov* et al. through a phenomenon termed 'tension-compression asymmetry' has been depicted. The phenomenon states that the polymeric entanglements in the hydrogels act as an additional junction point between the polymer chains and exert an elastic response under tension. These same active junction points become loose under compressive force, causing stress redistribution in the fiber network and causing deformation [59]. Although SNP incorporated Alg-GG hydrogels demonstrated slightly lower compressive modulus than the control group (Alg-GG-Silk sol.), the values are close to the determined compressive elastic modulus of native human articular cartilage, which is in the range of 240–1000 kPa [39].This makes our chosen Alg-GG nanocomposite hydrogel groups biomechanically suitable for articular cartilage differentiation.

The rheological analysis enabled us to print a large porous structure in the range of centimeter-scale with high printing attributes and printability. Whereas the polymeric bioink without the NPs (i.e., with Silk sol.) showed stability post-printing, the printing quality was less than the bioprinted constructs reinforced with the NPs. Printability value Pr = 1 denotes the highest printability when pores are created to have a square form. As shown in Fig. 6I, the ideal printability value was

observed with the bioink laden with native SNPs. One of the probable reasons for the less mean Pr values of the other two groups might be that hydrogels tend to spread when being extruded from the printing nozzle. Moreover, this minute discrepancy could have been brought on by either the minuscule variations in printing pressure or the somewhat quicker gelation brought on by post-crosslinking. However, the bioink with the native SNP acted as an adequate reinforcement to the Alg-GG bioink that helped improve the printability compared to the other groups.The same has been validated in previous studies where they demonstrated that the concentration of NPs is crucial in determining the mechanical enhancement of the bioprinted constructs post-printing [14].

Once the choice of the concentration of SNPs and the characterization of the printed constructs was validated, chondrogenesis studies in terms of Real-time PCR and H&E and immunofluorescence were achieved to comprehend if the hydrogel might support the development of a chondrocyte-specific matrix for future cartilage generation. In the current study, the TVA-BMSc cell line was embedded in the Alg-GG bioink containing various SNPs and Silk sol. to evaluate which experimental group imparts the best articular cartilage chondrogenesis. TVA-BMSc is a distinguished cell line, which earlier has demonstrated to preserve the BMSc characteristics beyond 40 passages during monolayer culture [22]. All three sets of the bioprinted construct exhibited expression of the genes for chondrogenesis, i.e., ACAN, SOX 9, and COL 2A1; however, the Alg-GG bioink with Silk sol. group reported enhanced chondrogenesis. Interestingly, the same group, i.e., Silk sol., displayed the least expression of the hypertrophic markers, i.e., COL X and MMP 13. The least expression of the YAP 1 gene in the Alg-GG bioink with the Silk sol. group indicated that this experimental set supports chondrogenesis since YAP negatively regulates the chondrogenesis of MSCs. Chondrogenesis requires YAP downregulation because chondrogenic signaling is repressed [60]. Although we have carried out the TAZ gene's gene expression, no expression was observed (hence no data was shown). One possible reason for this might be the issues with our primer. In our earlier study, we have manifested the role of SF-gelatin bioink in the downregulation of hypertrophic markers and upregulated expression of the articular chondrogenic marker [22]. Furthermore, we have also demonstrated its role in the upregulation of the Wnt signaling pathway in MSCs and primary chondrocytes [22,61]. The probable reason for this expression obtained with SF solution and not observed with its SNP counterpart is that all the cells encapsulated within the bioprinted construct might not be able to get in contact with the SNPs due to their heterogeneous distribution. In contrast, being in solution form, the Silk sol. within the bioink had a homogenous distribution and thus was accessible to the cells, which might have resulted in enhanced collagen production. Hence, the ability of these set of Alg-GG scaffold to facilitate chondrogenic redifferentiation was validated by the overexpression of cartilage-specific genes COL 2A1, SOX 9, and ACAN. New ECM formation within bioprinted construct was quantified biochemically by collagen II estimation. Collagen II is a significant constituent of the ECM of the cartilage that helps in the stabilization of the matrix. It constitutes 90–95% of the collagen (around 60% of the dry weight of the cartilage) in ECM and gives rise to interwoven fibrils with specific proteoglycans such as ACAN [40]. The bioprinted construct in our study, particularly with Silk sol., exhibited the highest collagen content on day 14. This imparts an excellent foundation for acquiring articular cartilage tissue with high collagen content [62]. Interaction between the ECM and the chondrocyte regulates various biological processes crucial for cartilage homeostasis [63]. The H&E images depicted homogenous distribution of the cells, especially in the Silk sol. group, as seen under fluorescence microscopy. The distinctive spherical morphology was confirmed on the day 14 culture period. The cell dispersion across the Alg-GG matrix was rather homogenous, and the cells retained some of the typical morphological traits and active division. One of the probable reasons for this is that the carbohydrate component of the GG, which includes a lot of 1,3-D-glucose and 1,4-D-glucose, can serve as a source of energy for the cells giving rise to the emergence of gaps within the hydrogel matrix and consequently leading to chondrocyte proliferation [64]. Apart from cellular distribution, developing a suitable ECM is critical to the functionality of the tissue-engineered construct. Immunofluorescence analysis confirmed upregulated collagen II expression at day 28 with the Silk sol. samples compared to the other two counterparts, further validating the gene expression results. These results were in accordance with the study carried out by Kim et al. [65], where they employed various lengths of silk fiber blended physically with GG hydrogel. Hence, our results distinctly depict that the Alg-GG bioink with SNPs or Silk sol. encapsulating MSCs was capable of depositing articular cartilage-like ECM, besides improving the printability and fidelity.

5. Conclusion

This study demonstrates the application of SNPs as rheology modifiers to the Alg-GG bioink, to improve the overall printability. A multicomponent shear-thinning bioink comprising Alg and GG was developed with good, rheological, biological, and adequate printing properties. Enhanced printability during printing and print fidelity post-crosslinking with $CaCl_2$ along with enhanced mechanical property was achieved with the native SNP compared to its regenerated SNP counterpart. The multicomponent bioink, containing SNP and encapsulated with TVA-BMSc, encouraged cellular growth and chondrogenic ECM formation. But the best articular chondrogenesis was achieved with the Alg-GG bioink containing the Silk sol. Thus, the SNPs could serve as a fundamental component of sophisticated materials in tissue engineering and personalized regenerative medicine and could be used in various systems.

CRediT authorship contribution statement

Juhi Chakraborty: Conceptualization, Methodology, Investigation, Writing – original draft, Data curation, Preparation of data, Writing – review & editing. **Nilotpal Majumder:** Investigation, Formal analysis, writing. **Aarushi Sharma:** Investigation. **Sukanya Prasad:** Conceptualization, Resources, Supervision, Funding acquisition, Validation, Writing – review & editing. **Sourabh Ghosh:** Conceptualization, Resources, Supervision, Funding acquisition, Validation, Writing – review & editing.

Declaration of competing interest

The authors declare that they have no known competing financial interests or personal relationships that could have appeared to influence the work reported in this paper.

Data availability

Data will be made available on request.

Acknowledgment

JC is grateful to the Department of Science and Technology (DST), India for the Inspire Fellowship (SRF) No. IF160365. We would like to thank Prof. Dr. Marcy Zenobi-Wong, ETH Zurich, Switzerland for her support during the initial part of the study.

Appendix A. Supplementary data

Supplementary data to this article can be found online at https://doi.org/10.1016/j.bprint.2022.e00232.

References

[1] S. Chawla, G. Desando, E. Gabusi, A. Sharma, D. Trucco, J. Chakraborty, C. Manferdini, M. Petretta, G. Lisignoli, S. Ghosh, The effect of silk-gelatin bioink

and TGF-β3 on mesenchymal stromal cells in 3D bioprinted chondrogenic constructs: a proteomic study, J. Mater. Res. (2021) 1–17, https://doi.org/10.1557/s43578-021-00230-5.
[2] D. Trucco, A. Sharma, C. Manferdini, E. Gabusi, M. Petretta, G. Desando, L. Ricotti, J. Chakraborty, S. Ghosh, G. Lisignoli, Modeling and fabrication of silk fibroin-gelatin-based constructs using extrusion-based three-dimensional bioprinting, ACS Biomater. Sci. Eng. 7 (2021) 3306–3320, https://doi.org/10.1021/acsbiomaterials.1c00410/suppl_file/ab1c00410_si_001.pdf.
[3] S. Kyle, Z.M. Jessop, A. Al-Sabah, I.S. Whitaker, 'Printability'' of candidate biomaterials for extrusion based 3D printing: state-of-the-art, ' Adv. Healthc. Mater. 6 (16) (2017), https://doi.org/10.1002/adhm.201700264.
[4] S. Hong, D. Sycks, H.F. Chan, S. Lin, G.P. Lopez, F. Guilak, K.W. Leong, X. Zhao, 3D printing of highly stretchable and tough hydrogels into complex, cellularized structures, Adv. Mater. 27 (2015) 4035–4040, https://doi.org/10.1002/adma.201501099.
[5] T. Huang, H. Xu, K. Jiao, L. Zhu, H.R. Brown, H. Wang, H.L. Wang, T. Huang, H. G. Xu, K.X. Jiao, L.P. Zhu, R. Brown, A novel hydrogel with high mechanical strength: a macromolecular microsphere composite hydrogel, Adv. Mater. 19 (2007) 1622–1626, https://doi.org/10.1002/adma.200602533.
[6] Y.H. Na, Double network hydrogels with extremely high toughness and their applications, KARJ 25 (2013) 185–196, https://doi.org/10.1007/S13367-013-0020-Y.
[7] K. Markstedt, A. Mantas, I. Tournier, H. Martínez Ávila, D. Hägg, P. Gatenholm, 3D bioprinting human chondrocytes with nanocellulose-alginate bioink for cartilage tissue engineering applications, Biomacromolecules 16 (2015) 1489–1496, https://doi.org/10.1021/acs.biomac.5b00188/asset/images/large/bm-2015-00188z_0007.jpeg.
[8] K.Y. Lee, D.J. Mooney, Alginate: properties and biomedical applications, Prog. Polym. Sci. 37 (2012) 106–126, https://doi.org/10.1016/J.progpolymsci.2011.06.003.
[9] T. Jeoh, D.E. Wong, S.A. Strobel, K. Hudnall, N.R. Pereira, K.A. Williams, B. M. Arbaugh, J.C. Cunniffe, H.B. Scher, How alginate properties influence in situ internal gelation in crosslinked alginate microcapsules (CLAMs) formed by spray drying, PLoS One 16 (2) (2021), https://doi.org/10.1371/journal.pone.0247171.
[10] C.J. Ferris, K.J. Gilmore, G.G. Wallace, M, In Het Panhuis, Modified gellan gum hydrogels for tissue engineering applications, Soft Matter 9 (2013) 3705–3711, https://doi.org/10.1039/c3sm27389J.
[11] A.M. Smith, R.M. Shelton, Y. Perrie, J.J. Harris, An initial evaluation of gellan gum as a material for tissue engineering applications, J. Biomater. Appl. 22 (2007) 241–254, https://doi.org/10.1177/0885328207076522.
[12] A.R. Akkineni, T. Ahlfeld, A. Funk, A. Waske, A. Lode, M. Gelinsky, Highly concentrated alginate-gellan gum composites for 3D plotting of complex tissue engineering scaffolds, Polymers 8 (2016) 170, https://doi.org/10.3390/polym8050170.
[13] M. Kesti, C. Eberhardt, G. Pagliccia, D. Kenkel, D. Grande, A. Boss, M. Zenobi-Wong, Bioprinting complex cartilaginous structures with clinically compliant biomaterials, Adv. Funct. Mater. 25 (2015) 7406–7417, https://doi.org/10.1002/adfm.201503423.
[14] M. Lee, K. Bae, P. Guillon, J. Chang, Ø. Arlov, M. Zenobi-Wong, Exploitation of cationic silica nanoparticles for bioprinting of large-scale constructs with high printing fidelity, ACS Appl. Mater. Interfaces 10 (2018) 37820–37828, https://doi.org/10.1021/acsami.8b13166/suppl_file/am8b13166_si_003.avi.
[15] N. Bhardwaj, R. Rajkhowa, X. Wang, D. Devi, Milled non-mulberry silk fibroin microparticles as biomaterial for biomedical applications, Int. J. Biol. Macromol. 81 (2015) 31–40, https://doi.org/10.1016/j.ijbiomac.2015.07.049.
[16] C. Vyas, J. Zhang, Ø. Øvrebø, B. Huang, I. Roberts, M. Setty, B. Allardyce, H. Haugen, R. Rajkhowa, P. Bartolo, 3D printing of silk microparticle reinforced polycaprolactone scaffolds for tissue engineering applications, Mater. Sci. Eng. C. 118 (2021), 111433, https://doi.org/10.1016/j.msec.2020.111433.
[17] J.I. Solomun, J.D. Totten, T. Wongpinyochit, A.J. Florence, F.P. Seib, Manual versus microfluidic-assisted nanoparticle manufacture: impact of silk fibroin stock on nanoparticle characteristics, ACS Biomater. Sci. Eng. 6 (2020) 2796–2804, https://doi.org/10.1021/acsbiomaterials.0c00202/suppl_file/ab0c00202_si_001.pdf.
[18] X. Chen, Z. Shao, D.P. Knight, F. Vollrath, Conformation transition kinetics of Bombyx mori silk protein, Proteins 68 (2007) 223–231, https://doi.org/10.1002/prot.21414.
[19] A.S. Lammel, X. Hu, S.H. Park, D.L. Kaplan, T.R. Scheibel, Controlling silk fibroin particle features for drug delivery, Biomaterials 31 (2010) 4583–4591, https://doi.org/10.1016/J.biomaterials.2010.02.024.
[20] M. Bhattacharjee, S. Chawla, S. Chameettachal, S. Murab, N.S. Bhavesh, S. Ghosh, Role of chondroitin sulphate tethered silk scaffold in cartilaginous disc tissue regeneration, Biomed, Materials 11 (2) (2016), 025014, https://doi.org/10.1088/1748-6041/11/2/025014.
[21] S. Murab, J. Samal, A. Shrivastava, A.R. Ray, A. Pandit, S. Ghosh, Glucosamine loaded injectable silk-in-silk integrated system modulate mechanical properties in bovine ex-vivo degenerated intervertebral disc model, Biomaterials 55 (2015) 64–83, https://doi.org/10.1016/j.biomaterials.2015.03.032.
[22] S. Chawla, A. Kumar, P. Admane, A. Bandyopadhyay, S. Ghosh, Elucidating role of silk-gelatin bioink to recapitulate articular cartilage differentiation in 3D bioprinted constructs, Bioprinting 7 (2017) 1–13, https://doi.org/10.1016/j.bprint.2017.05.001.
[23] E.S. Gil, D.J. Frankowski, R.J. Spontak, S.M. Hudson, Swelling behavior and morphological evolution of mixed gelatin/silk fibroin hydrogels, Biomacromolecules 6 (2005) 3079–3087, https://doi.org/10.1021/BM050396C.
[24] X. Hu, D. Kaplan, P. Cebe, Determining beta-sheet crystallinity in fibrous proteins by thermal analysis and infrared spectroscopy, Macromolecules 39 (2006) 6161–6170, https://doi.org/10.1021/ma0610109/asset/images/large/ma0610109f00006.jpeg.
[25] P. Dubey, S. Seit, P.K. Chowdhury, S. Ghosh, Effect of macromolecular crowders on the self-assembly process of silk fibroin, Macromol. Chem. Phys. 221 (2020), 2000113, https://doi.org/10.1002/MACP.202000113.
[26] C.C. Piras, D.K. Smith, Multicomponent polysaccharide alginate-based bioinks, J. Mater. Chem. B. 8 (2020) 8171–8188, https://doi.org/10.1039/D0TB01005G.
[27] J. Chakraborty, S. Roy, S. Ghosh, Biomedical Materials 3D printed hydroxyapatite promotes congruent bone ingrowth in rat load bearing defects, Biomed. Mater. 17 (2022), 35008, https://doi.org/10.1088/1748-605X/ac6471.
[28] A.B. Kakarla, I. Kong, C. Kong, H. Irving, Extrusion-based bioprinted boron nitride nanotubes reinforced alginate scaffolds: mechanical, Printabil. and Cell Viabil. Eval. 14 (3) (2022) 486, https://doi.org/10.3390/polym14030486.
[29] C. Guo, C. Li, H.V. Vu, P. Hanna, A. Lechtig, Y. Qiu, X. Mu, S. Ling, A. Nazarian, S. J. Lin, D.L. Kaplan, Thermoplastic moulding of regenerated silk, Nat. Mater. 191 (2019) 19, https://doi.org/10.1038/s41563-019-0560-8 (2019) 102–108.
[30] S. Midha, S. Chawla, J. Chakraborty, S. Chameettachal, S. Ghosh, Differential regulation of hedgehog and parathyroid signaling in mulberry and nonmulberry silk fibroin textile braids, ACS Biomater. Sci. Eng. 4 (2018) 595–607, https://doi.org/10.1021/acsbiomaterials.7b00874/asset/images/medium/ab-2017-00874e_0008.gif.
[31] P. Admane, A.C. Gupta, P. Jois, S. Roy, C. Lakshmanan, G. Kalsi, B. Bandyopadhyay, S. Ghosh, Direct 3D Bioprinted Full-Thickness Skin Constructs Recapitulate Regulatory Signaling Pathways and Physiology of Human Skin, vol. 15, 2019, e00051, https://doi.org/10.1016/j.bprint.2019.e00051.
[32] S. Azarmi, Y. Huang, H. Chen, S. McQuarrie, D. Abrams, W. Roa, W.H. Finlay, G. G. Miller, R. Löbenberg, Optimization of a two-step desolvation method for preparing gelatin nanoparticles and cell uptake studies in 143B osteosarcoma cancer cells, J. Pharm. Pharmaceut. Sci. 9 (1) (2006) 124–132.
[33] A. Mahajan, E. Ramana, Patents on magnetoelectric multiferroics and their processing by electrophoretic deposition, recent patents mater, Sci 7 (2014) 109–130, https://doi.org/10.2174/1874464807666140701190424.
[34] R. Sharma, U. Sharma, Formulation and characterization of atenolol-loaded gellan gum nanoparticles, Indian J. Pharmaceut. Sci. 83 (2021) 60–65, https://doi.org/10.36468/pharmaceutical-sciences.750.
[35] S. Das, F. Pati, S. Chameettachal, S. Pahwa, A.R. Ray, S. Dhara, S. Ghosh, Enhanced redifferentiation of chondrocytes on microperiodic silk/gelatin scaffolds: toward tailor-made tissue engineering, Biomacromolecules 14 (2013) 311–321, https://doi.org/10.1021/bm301193t/suppl_file/bm301193t_si_001.pdf.
[36] P. Dubey, S. Murab, S. Karmakar, P.K. Chowdhury, S. Ghosh, Modulation of self-assembly process of fibroin: an insight for regulating the conformation of silk biomaterials, Biomacromolecules 16 (2015) 3936–3944, https://doi.org/10.1021/acs.biomac.5b01258.
[37] N.D. Lazo, D.T. Downing, Crystalline regions of Bombyx mori silk fibroin may exhibit β-turn and β-helix conformations, Macromolecules 32 (1999) 4700–4705, https://doi.org/10.1021/MA9900582/asset/images/large/ma9900582f00006.jpeg.
[38] D. Petta, A.R. Armiento, D. Grijpma, M. Alini, D. Eglin, M. D'Este, 3D bioprinting of a hyaluronan bioink through enzymatic-and visible light-crosslinking, Biofabrication 10 (4) (2018), 044104, https://doi.org/10.1088/1758-5090/AADF58.
[39] E.C. Beck, M. Barragan, M.H. Tadros, S.H. Gehrke, M.S. Detamore, Approaching the compressive modulus of articular cartilage with a decellularized cartilage-based hydrogel, Acta Biomater. 38 (2016) 94–105, https://doi.org/10.1016/j.actbio.2016.04.019.
[40] H. Akkiraju, A. Nohe, Role of chondrocytes in cartilage formation, progression of osteoarthritis and cartilage regeneration, J. Dev. Biol. 3 (2015) 177, https://doi.org/10.3390/JDB3040177.
[41] J. Sun, H. Tan, Alginate-based biomaterials for regenerative medicine applications, Mater. (Basel, Switzerland) 6 (2013) 1285–1309, https://doi.org/10.3390/MA6041285.
[42] T. Osmałek, A. Froelich, S. Tasarek, Application of gellan gum in pharmacy and medicine, Int. J. Pharm. 466 (2014) 328–340, https://doi.org/10.1016/J.IJPHARM.2014.03.038.
[43] S. Honary, F. Zahir, Effect of zeta potential on the properties of nano-drug delivery systems - a review (Part 1), Trop. J. Pharmaceut. Res. 12 (2013) 255–264, https://doi.org/10.4314/TJPR.V12I2.19.
[44] B. Yameen, W. Il Choi, C. Vilos, A. Swami, J. Shi, O.C. Farokhzad, Insight into nanoparticle cellular uptake and intracellular targeting, J. Contr. Release 190 (2014) 485–499, https://doi.org/10.1016/j.jconrel.2014.06.038.
[45] R. Vogel, A.K. Pal, S. Jambhrunkar, P. Patel, S.S. Thakur, E. Reátegui, H.S. Parekh, P. Saá, A. Stassinopoulos, M.F. Broom, High-resolution single particle zeta potential characterisation of biological nanoparticles using tunable resistive pulse sensing, Sci. Rep. 7 (1) (2017), https://doi.org/10.1038/S41598-017-14981-X.
[46] S.H. Brewer, W.R. Glomm, M.C. Johnson, M.K. Knag, S. Franzen, Probing BSA binding to citrate-coated gold nanoparticles and surfaces, Langmuir 21 (2005) 9303–9307, https://doi.org/10.1021/la050588t/asset/images/large/la050588tf00003.jpeg.
[47] F.J. González-Fuentes, G.A. Molina, R. Silva, J.L. López-Miranda, R. Esparza, A. R. Hernandez-Martinez, M. Estevez, Developing a CNT-SPE sensing platform based on green synthesized AuNPs, using sargassum sp, Sensors 20 (2020) 6108, https://doi.org/10.3390/S20216108.
[48] M. Danaei, M. Dehghankhold, S. Ataei, F. Hasanzadeh Davarani, R. Javanmard, A. Dokhani, S. Khorasani, M.R. Mozafari, Impact of particle size and polydispersity

index on the clinical applications of lipidic nanocarrier systems, Pharmaceutics 10 (2) (2018), https://doi.org/10.3390/pharmaceutics10020057.
[49] A.A. Lozano-Pérez, M.G. Montalbán, S.D. Aznar-Cervantes, F. Cragnolini, J. L. Cenis, G. Víllora, Production of silk fibroin nanoparticles using ionic liquids and high-power ultrasounds, J. Appl. Polym. Sci. 132 (12) (2015), https://doi.org/10.1002/APP.41702.
[50] V. Forest, J. Pourchez, Preferential binding of positive nanoparticles on cell membranes is due to electrostatic interactions: a too simplistic explanation that does not take into account the nanoparticle protein corona, Mater. Sci. Eng. C. 70 (2017) 889–896, https://doi.org/10.1016/j.msec.2016.09.016.
[51] M. Samie, N. Muhammad, M.A. Yameen, A.A. Chaudhry, H. Khalid, A.F. Khan, Aqueous solution of a basic ionic liquid: a perspective solvent for extraction and regeneration of silk powder from Bombyx mori silk cocoons, J. Polym. Environ. 28 (2020) 657–667, https://doi.org/10.1007/S10924-019-01634-5/figures/12.
[52] H. Herrada-Manchón, D. Rodríguez-González, M.A. Fernández, N.W. Kucko, F. B. De Groot, E. Aguilar, Effect on rheological properties and 3D printability of biphasic calcium phosphate microporous particles in hydrocolloid-based hydrogels, Gels (Basel, Switzerland) 8 (1) (2022), https://doi.org/10.3390/GELS8010028.
[53] S. Mueller, E.W. Llewellin, H.M. Mader, The rheology of suspensions of solid particles, Proc. R. Soc. A Math. Phys. Eng. Sci. 466 (2010) 1201–1228, https://doi.org/10.1098/RSPA.2009.0445.
[54] S. Chawla, S. Midha, A. Sharma, S. Ghosh, Silk-based bioinks for 3D bioprinting, Adv. Healthc. Mater. 7 (8) (2018), e1701204, https://doi.org/10.1002/adhm.201701204.
[55] S.G. Marapureddy, P. Hivare, A. Sharma, J. Chakraborty, S. Ghosh, S. Gupta, P. Thareja, Rheology and direct write printing of chitosan - graphene oxide nanocomposite hydrogels for differentiation of neuroblastoma cells, Carbohydr. Polym. 269 (2021), 118254, https://doi.org/10.1016/J.CARBPOL.2021.118254.
[56] A. Chakraborty, A. Roy, S.P. Ravi, A. Paul, Exploiting the role of nanoparticles for use in hydrogel-based bioprinting applications: concept, design, and recent advances, Biomater. Sci. 9 (2021) 6337–6354, https://doi.org/10.1039/D1BM00605C.
[57] L. Wang, Z. Luo, Q. Zhang, Y. Guan, J. Cai, R. You, X. Li, Effect of degumming methods on the degradation behavior of silk fibroin biomaterials, Fibers Polym. 20 (2019) 45–50, https://doi.org/10.1007/S12221-019-8658-9, 2019 201.
[58] C.W. Peak, J. Stein, K.A. Gold, A.K. Gaharwar, Nanoengineered colloidal inks for 3D bioprinting, Langmuir 34 (2018) 917–925, https://doi.org/10.1021/acs.langmuir.7b02540/asset/images/large/la-2017-02540z_0005.jpeg.
[59] A.D. Drozdov, J.C. de Christiansen, Tension–compression asymmetry in the mechanical response of hydrogels, J. Mech. Behav. Biomed. Mater. 110 (2020), 103851, https://doi.org/10.1016/j.jmbbm.2020.103851.
[60] A. Karystinou, A.J. Roelofs, A. Neve, F.P. Cantatore, H. Wackerhage, C. De Bari, Yes-associated protein (YAP) is a negative regulator of chondrogenesis in mesenchymal stem cells, Arthritis Res. Ther. 17 (1) (2015), https://doi.org/10.1186/S13075-015-0639-9.
[61] J. Chakraborty, S. Ghosh, Cellular proliferation, self-assembly, and modulation of signaling pathways in silk fibroin gelatin-based 3D bioprinted constructs, ACS Appl. Bio Mater. 3 (2020) 8309–8320, https://doi.org/10.1021/acsabm.0c01252/asset/images/acsabm.0c01252.social.jpeg_v03.
[62] L. Roseti, C. Cavallo, G. Desando, V. Parisi, M. Petretta, I. Bartolotti, B. Grigolo, Three-Dimensional bioprinting of cartilage by the use of stem cells: a strategy to improve regeneration, Mater. (Basel, Switzerland) 11 (9) (2018), https://doi.org/10.3390/MA11091749.
[63] R.F. Loeser, Integrins and chondrocyte–matrix interactions in articular cartilage, Matrix Biol. 39 (2014) 11–16, https://doi.org/10.1016/j.matbio.2014.08.007.
[64] J.T. Oliveira, T.C. Santos, L. Martins, R. Picciochi, A.P. Marques, A.G. Castro, N. M. Neves, J.F. Mano, R.L. Reis, Gellan gum injectable hydrogels for cartilage tissue engineering applications: in vitro studies and preliminary in vivo evaluation, Tissue Eng. 16 (2010) 343–353, https://doi.org/10.1089/ten.tea.2009.0117.
[65] W. Kim, | Joo, H. Choi, P. Kim, J. Youn, | Jeong, E. Song, A. Motta, C. Migliaresi, | Gilson Khang, G. Khang, Preparation and evaluation of gellan gum hydrogel reinforced with silk fibers with enhanced mechanical and biological properties for cartilage tissue engineering,15(11) (2021) 936-947 . https://doi.org/10.1002/term.3237.